NASA-CR-200910

aer ATMOSPHERIC AND ENVIRONMENTAL RESEARCH, INC.

Dr. Yogesh Sud
Code 913
NASA Goddard Space Flight Center
Greenbelt, MD 20771

Re: Second progress report, contract NAS 5-32861 (AER Project P602)

Dear Dr. Sud:

This report, prepared by Atmospheric and Environmental Research, Inc., covers progress during the period since September 1995 under the subject contract.

1. Activities during reporting period

We continued our assessments of the NASA Goddard Earth Observing System-1 Data Assimilation System (GEOS-1 DAS), regarding energetics and angular momentum quantities. The energetics diagnostics, in particular, are useful in determining a measure of the types of climate signals during the multi-year period already analyzed as part of the GEOS DAS-1 reanalysis effort. For example, we see a distinct difference in the zonal mean and in the eddy kinetic energy terms between a year featuring a warm Pacific water El Niño event (1987) and one that had a cold La Niña event (1988). We presented some of our results concerning this topic at the Annual NOAA Climate Diagnostics Workshop in November 1995, in a presentation entitled, "Angular momentum and energetics in reanalysis products." There we focused on comparisons of the NASA EOS DAS-1 system with the NOAA NCEP/NCAR Reanalysis Project. Some of the differences in the energetics terms led us to conclude that the mean zonal winds and eddy terms had considerable differences. A copy of the relevant Proceedings contribution from this workshop is enclosed.

In a related vein, we have compared the heating rates from the GEOS DAS-1 with values of outgoing longwave radiation for an eight-year period. We find, in particular, that there is considerable correlation in the west central Pacific between (negative) heating and vertically averaged latent heating. Information concerning these comparison is addressed in Attachment 1.

We have also examined two aspects of assessments of model behavior from the Atmospheric Model Intercomparison Project, in which two Goddard general circulation models participate. As one aspect, we focused on angular momentum statistics, for which we have verified the whole suite of AMIP models. The models simulate global angular momentum quite well in general on the mean and on seasonal time scales, but a little less successfully on interannual time scales. We co-authored a manuscript, entitled

840 MEMORIAL DRIVE, CAMBRIDGE, MA 02139-3794
TEL: (617) 547-6207 FAX: (617) 661-6479

"Atmospheric angular momentum fluctuations in global circulation models during the period 1979-1988," which was submitted for publication (Copy enclosed). We have also examined issues of water vapor and its transports from AMIP models, and from observations . We find that the models are relatively successful on seasonal time scales, but much less so on interannual scales. We are co-authoring a manuscript as well on this aspect of AMIP verification, which will be submitted for publication soon.

We have a new staff member who will help us on this project: Dr. Haig Iskenderian has just joined AER as a Postdoctoral Fellow, and he will spend part of his time contributing to the issues of the reported project.

2. Plans for upcoming period

We will extend our studies of NASA runs that include the effects of tropical deforestation, and we plan to prepare a paper on the impact of such physical parameterization changes on global diagnostics. We will keep up our GEOS energetics and angular momentum studies, with additional years of analyses, now being produced, to assess the climatic implications of the signals, and we will continue comparisons with other data sets, such as the NCEP/NCAR reanalyses.

Sincerely yours,

David A. Salstein

David A. Salstein
Principal Investigator

3 enclosures

cc: Contracting Officer, Code 289, 1 copy
Center for AeroSpace Information, 2 copies

April 23, 1996

ATMOSPHERIC ANGULAR MOMENTUM FLUCTUATIONS IN GLOBAL CIRCULATION MODELS DURING THE PERIOD 1979-1988

by

R. Hide[1,3]
J. O. Dickey and S. L. Marcus[1]
R. D. Rosen and D. A. Salstein[2]

[1] Space Geodetic Science and Applications Group
Jet Propulsion Laboratory,
California Institute of Technology,
4800 Oak Grove Drive
Pasadena, California 91109-8099, USA.
Tel: 818-354-3235; Fax: 818-393-6890

[2] Atmospheric and Environmental Research Inc. (AER)
840 Memorial Drive
Cambridge, Massachusetts 02139, USA.
Tel: 617-547-6207; Fax: 617-661-6479

[3] Department of Physics (Atmospheric, Oceanic and Planetary Physics)
University of Oxford
Clarendon Laboratory, Parks Road,
Oxford OX1 3PU England, UK.
Tel: 0-1865-272086; Fax: 0-1865-272924

Submitted to JGR-Atmospheres

ABSTRACT

Changes in major global dynamical phenomena in the Earth's atmosphere are manifested in the time series of atmospheric angular momentum (AAM), as determined directly from meteorological observations and indirectly from geodetic observations of small fluctuations in the rotation of the solid Earth that are proportional to length of day (LOD). AAM fluctuations are intimately linked with energetic processes throughout the whole atmosphere, and also with the stresses at the Earth's surface produced largely by turbulent momentum transport in the oceanic and continental boundary layers and by the action of normal pressure forces on orographic features. A stringent test of any numerical global circulation model (GCM) is therefore provided by a quantitative assessment of its ability to represent AAM fluctuations on all relevant time scales, ranging from months to several years. From monthly data provided by the Atmospheric Model Intercomparison Project (AMIP) of the World Climate Research Programme (WCRP), we have investigated seasonal and interannual fluctuations and the decadal mean in the axial component of AAM in 23 AMIP GCMs over the period 1979-1988. The decadal means are generally well simulated, with the model median value (1.58×10^{26} kg m^2 s^{-1}) being only 3.5% larger than the observed mean and with 10 of the models being within 5% of the observed. The seasonal cycle is well reproduced, with the median amplitude of the models' seasonal standard deviations being only 2.4% larger than observed. Half the seasonal amplitudes lie within 15% of the observed and the median correlation found between the observed and model seasonal cycles is 0.95. The dominant seasonal error is an underestimation of AAM during northern hemisphere winter associated with errors in the position of subtropical jets. Less robust are the modeled interannual variations, though the median correlation of 0.61 between model simulation and observed AAM is statistically significant. The two El Niño-Southern Oscillation (ENSO) events that occurred during the AMIP decade 1979-1988 have the expected positive AAM anomalies though the AAM signature of the 1982-1983 event tends to be underestimated, and that of the 1986-1987 event overestimated.

1. INTRODUCTION

The Earth's atmosphere super-rotates relative to the underlying planet such that, if transferred to the solid Earth below, the angular momentum associated with this super-rotation would reduce the length of the day (LOD) by around 3 milliseconds. Geodetic observations going back several decades reveal irregular LOD fluctuations of up to about 1 ms on interannual, seasonal and intraseasonal time scales (see Fig. 1), and detailed studies using modern meteorological and geodetic data have established that

Figure 1 near here

these fluctuations are largely of meteorological origin (for reviews, see Hide and Dickey, 1991; Rosen, 1993; Dickey 1993; Eubanks, 1993 and references therein). Fluctuations in the equatorial components of atmospheric angular momentum (see Appendix A) are associated with non-axisymmetric features of the global atmospheric circulation and make a substantial contribution to polar motion (the observed wobble of the rotation axis of the solid Earth with respect to geographical coordinates) on sub-decadal time scales. On decadal and longer time scales [Fig. 1(b)], the dominant forcing is due to non-meteorological agencies, including angular momentum exchange between Earth's liquid metallic core and the overlying solid mantle and "spin-orbit" coupling between Earth and Moon largely associated with tidal friction in the oceans. The angular momentum of the oceans is not well determined owing to the paucity of data; however, fluctuations in magnitude in their axial component are no more than 10% of those of the axial component of AAM (hereafter used as an abbreviation for the axial component of atmospheric angular momentum) with which this paper is concerned.

The task of improving the performance of numerical models of the atmosphere by identifying and correcting weaknesses in their formulation requires systematic methods for testing model performance. The inclusion of diagnostics based on analyses and forecasts of AAM offers several advantages. The most obvious is the unique opportunity it provides, in principle at least, for comparing on a clear-cut physical basis the output of a global quantity from the models with observations that are completely independent of meteorological data, namely those of short-term fluctuations in the LOD. The axial torques at the Earth's surface responsible for meteorologically-induced fluctuations in the Earth's rotation are produced by (a) tangential stresses in turbulent boundary layers and (b) normal (pressure) stresses acting on irregular topography. These stresses are transmitted directly to the solid Earth over continental regions and indirectly over the oceans.

Secondly, considerations of AAM fluctuations bear directly on fundamental aspects of the energetics of the global atmospheric circulation and cannot be separated from them. In the absence of energy sources, the atmosphere would rotate with the solid Earth like a rigid body (i.e., no winds), for this would be a state of minimum kinetic energy of the whole system for a given total angular momentum. Differential solar heating produces atmospheric winds, the kinetic energy of which derives from the available potential energy of the atmosphere (associated with gravity acting on the density field maintained by the heating) through the action of vertical motions. Angular momentum is thereby redistributed without any change occurring in the total amount in the whole system (since solar heating produces no net torque) but with an increase in the total kinetic energy. A substantial contribution to this energy is associated with 'super-rotation' of the atmosphere at an average azimuthal wind speed U (say) of about 7 ms^{-1}, namely $\frac{1}{2} MU^2$ if M is the total mass of the atmosphere. Observed fluctuations in AAM amount to a considerable fraction of the mean $MU\bar{R}$ in magnitude (where $\bar{R}$ is the mean radius of the solid Earth). Concomitant fluctuations in the kinetic energy associated with the super-rotation amount to a considerable fraction of the mean $\frac{1}{2} MU^2$. By energy conservation arguments, these can only be produced by dynamical processes involving nonlinear interactions between the zonal wind field, the non-zonal wind field, and the field of available potential energy in the atmosphere. Successful models of the global circulation of the atmosphere must of course represent these interactions correctly. (For further details see Bell *et al.*, 1991.)

Thanks to the First GARP Global Experiment (FGGE) of the Global Atmospheric Research Programme (GARP) it became possible to obtain useful daily determinations of the total AAM for comparison with geodetic data on LOD variations [Hide *et al.*, 1980]. Manifold subsequent developments following this early work include practical arrangements for producing and disseminating routine daily or more frequent determinations not only of the axial component of the AAM vector but also of the equatorial components [Barnes *et al.*, 1983; Salstein *et al.*, 1993]. These determinations (see Appendix A, equations A7 to A9) are now made from analysis (and in some cases also from forecast) fields by several meteorological centers, namely the European Centre for Medium-Range Weather Forecasts (ECMWF), Japanese Meteorological Agency (JMA), United Kingdom Meteorological Office (UKMO), and United States National Meteorological Center (NMC, recently renamed National Centers for Environmental Prediction, NCEP). Plans are now in hand at some centers for producing routine determinations of surface torques, which will supplement the AAM data and facilitate diagnostic studies.

The ambitious Atmospheric Model Intercomparison Project (AMIP) of the World Climate Research Programme (WCRP) is one of the main activities initiated by the WCRP's Working Group on Numerical Experimentation (WGNE) in its efforts to refine atmospheric models and improve their ability to produce useful forecasts of changes in weather and climate [Gates, 1992]. Thirty atmospheric modeling groups cooperate unselfishly in AMIP, together with more than twenty groups engaged in diagnostics subprojects of AMIP concerned with the thorough testing of models by means of quantitative intercomparisons of their ability to reproduce various aspects of the behavior of the atmosphere. Our efforts in the atmospheric angular momentum diagnostics subproject of AMIP bear directly on the extent to which zonal winds and the exchange of angular momentum between the atmosphere and the underlying planet are represented correctly by the models being tested.

Specific dynamical phenomena produce strong signatures in observed AAM fluctuations and the study of the angular momentum balance of the Earth-atmosphere-ocean system is relevant to many climate dynamics issues. Earth rotation variations provide a unique and truly global measure of changes in the atmosphere, oceans, and cryosphere, on time scales ranging from days to centuries. The variation of AAM has now been convincingly linked to sub-decadal changes in the length-of-day down to time scales of about a week [Dickey *et al.*, 1992]. The axial component of the total AAM shows a characteristic seasonal variation and pronounced 'broad-band' intraseasonal fluctuations [Figs. 1(d) and (e)]. Oscillations on intraseasonal time scales, including those related to the Madden-Julian oscillation, have been shown to involve AAM changes propagating within the tropics [Anderson and Rosen, 1983], with contributions from orographically-forced oscillations in the extratropics [Dickey *et al.*, 1991 and Marcus *et al.*, 1994]. The accurate characterization of the seasonal AAM cycle involves the whole atmosphere from 1000 to 1 mb, with stratospheric winds making a significant contribution [Rosen and Salstein, 1985; and Dickey *et al.*, 1994].

LOD and AAM also exhibit interannual variations, on quasi-biennial and quasi-quadrennial time scales [Chao, 1984, 1988, 1989; Dickey *et al.*, 1992, 1994; Eubanks *et al.*, 1986; Jordi *et al.*, 1995; and Salstein and Rosen, 1986-see Fig. 1(c)]. Well-correlated with ENSO events, these are associated with large-scale zonal-wind anomalies which appear to propagate from tropical to extra-tropical regions [Dickey *et al.*, 1992; Salstein *et al.*, 1993]. Teleconnections between different latitude bands have been discovered in AAM data on these time scales, providing insights into the global structure of interannual climate variations [Dickey *et al.*, 1992; Salstein *et al.*, 1993; and Marcus and Dickey, 1994]. Indeed, much progress has been made during the past twenty years with the investigation of AAM fluctuations on sub-decadal time scales. Important new results can be expected from future studies, including numerical simulations of AAM fluctuations on decadal and longer time scales. Such studies, in addition to their intrinsic interest in meteorology and oceanography, will indirectly facilitate investigations of angular momentum exchange between the Earth's liquid metallic outer core and overlying mantle and other non-meteorological processes which, though evidently relatively unimportant on sub-decadal time scales in the excitation of irregular fluctuations in the Earth's rotation, play dominant roles on longer time scales.

The data used and methodology employed in our study are outlined in Section 2, setting the scene for the axial AAM intercomparisons of decadal means and on seasonal and interannual time scales, presented and summarized in Section 3 and 4. In the future work it will be important to investigate the extent to which atmospheric models can reproduce fluctuations in the equatorial components of atmospheric angular momentum. These excite measurable movements in the Earth's pole of rotation on sub-decadal time scales, including a Chandlerian free wobble with a period of 14 months (see Appendix A).

2. DATA AND METHODOLOGY

a. Observed values of angular momentum

The most complete series of AAM and zonal wind fields generally available for the AMIP decade (1979-1988) are those produced operationally by the NMC. Comparisons of the NMC AAM series with one from the ECMWF [Rosen *et al.*, 1987; Rosen, 1993; Dickey *et al.*, 1993] indicate that the differences between the two series are so small that we can confidently use either for validating the AMIP model results. Up to twice-daily values of zonal-mean zonal wind $[u]$ from the NMC have been archived on a 2.5° latitude grid at standard pressure levels between 1000 and 50 mb. We created monthly mean fields of $[u]$ by averaging all data available within each calendar month during 1979-1988. These fields were then used to create a monthly series of the relative angular momentum (M^w) of the atmosphere about the polar axis by applying equation (A13) and evaluating

$$M^w = 2\pi \overline{R}^3 g^{-1} \int_{50}^{1000} \int_{-\pi/2}^{\pi/2} [u] \cos^2 \phi \, d\phi \, dp. \tag{2.1}$$

In addition to the global M^w values, we also computed the relative angular momentum of the atmosphere in each of 46 equal-area belts (m_b^w) over the globe to help isolate regional sources of model errors in (m_b^w). As explained by Rosen and Salstein [1983], the number of belts is dictated by the 2.5° latitude resolution of the NMC analyses and the constraint that all belts should have the same area as that between the equator and 2.5°N. The latitudinal boundaries of the resulting 46 belts are listed by Rosen and Salstein [1983]. Within each belt, m_b^w is given by

$$m_b^w = 2\pi \overline{R}^3 g^{-1} \int_b \int_{50}^{1000} [u] \cos^2 \phi \, d\phi \, dp, \tag{2.2}$$

where ϕ runs between the southern and northern boundaries of belt b. In evaluating this expression numerically, care was taken to ensure that $\sum_{46 \text{ belts}} m_b^w = M^w$ is satisfied each month. Although the creation of m_b^w values precludes consideration of variability within a vertical column, the results of Rosen and Salstein [1983] suggest that such variability is often more coherent than that in the meridional direction. To maintain a manageably-sized regional data set, therefore, we feel it sufficient to limit the bulk of our intra-global analyses here to m_b^w.

b. Model values of angular momentum

Monthly mean values of $[u]$ were available from 29 GCMs at the time of writing as part of the standard output archived by AMIP [Gates, 1992]. All but 5 of the GCMs include pressure levels up to 50 mb, and these 5 models were eliminated from further consideration to maintain consistency with the depth of the atmosphere in the NMC observations.[1] By the same token, levels above 50 mb that may have been available for an AMIP model are disregarded here. The model values of $[u]$ are given on two-dimensional latitude-pressure grids whose resolutions vary from model to model. To simplify computations, however, we interpolated all model output to the same 2.5° latitude grid as the NMC observations, although we retained each model's archived distribution of pressure levels when computing M^w and m_b^w.

Model results shown here are identified by the acronyms defined by Gates [1992], as updated by Phillips [1994] (see Table 1).[2] The latter report summarizes the major characteristics of each AMIP model, and no attempt to reproduce that information in any detail is made here. It is clear from this documentation, however, that the set of AMIP models is heterogeneous, embodying a wide range of choices in resolution and physical parameterizations; hence an assumption that the relatively small sample of M^w values available to us is drawn from a statistically normal population is not justified. We, therefore, avoid using the mean and standard deviation as measures of central tendency and spread, respectively, of the distribution of model M^w values. Instead, we use the median and the interquartile range (IQR) described by Lanzante [1996] for these statistics. The IQR is simply the difference defined by the upper quartile minus the lower quartile of values in the distribution; i.e., it measures the distance spanned by the middle half of the distribution. An advantage of the IQR is that it is relatively resistant to the presence of large outliers, unlike the standard deviation. For a Gaussian distribution, however, the two statistics are related: in this case the IQR is 1.349 times the standard deviation [Lanzante, 1996].

[1]Output from GISS was also disregarded, because of its unusual vertical distribution.
[2]An exception is the SUNYA/NCAR model, which we abbreviate as SNG.

c. Temporal decomposition

Rosen *et al.* [1991b] and Hide and Dickey [1991] illustrate that the temporal variability in the Earth-atmosphere system can be usefully separated into three frequency bands: intraseasonal, seasonal, and interannual. A decomposition for LOD, which also experiences substantial decadal variability due to core-mantle interaction, is shown in Fig. 1. The seasonal cycle is by far the dominant sub-decadal signal, being ~1ms in peak to peak amplitude and typically explaining more than 75% of the variance in the total series [see Fig. 1(a)]. Hence, our inability to consider intraseasonal variations in M^w here [Fig. 1(e)] because of the monthly mean resolution of the AMIP standard output is not overly limiting. To define the seasonal component of each of the model and observed M^w series, we first removed their decadal means, i.e., the average of the 120 monthly values for 1979-1988, and then averaged the 10 values for each calendar month. An interannual component, which is considerably smaller than the annual signature, is formed by averaging the monthly values in each of the 40 "seasons" during the decade, beginning with January-March 1979, and subtracting from this series the decadal mean seasonal cycle. Although this "interannual" component includes some higher (non-seasonal) frequency variability, we will see that the bulk of its variance is from time scales longer than a year. Hence the term "interannual" is appropriate for this component.

In the next section, we compare the decadal mean, seasonal, and interannual components of the 23 model M^w series with the observed components obtained from the NMC analyses. As noted above, the accuracy of the NMC analyses is not a significant issue here; the differences found among the model M^w series are typically much larger than the uncertainty in the observed series.

3. RESULTS

Time series of M^w for each of the 23 AMIP models are shown in Figure 2 (solid lines)

Figure 2 near here

and are contrasted with M^w determined from the operational NMC analysis (dashed lines) and that inferred from geodetic data (dotted lines). The observed AAM and LOD track each other with a high degree of fidelity, although the amplitude of the annual and interannual components of the observed AAM are somewhat under-estimated relative to the LOD, partly because of neglect of the atmosphere above 50mb [Rosen and Salstein. 1985 and Dickey *et al.*, 1994]. The overall agreement between the simulated and observed results is fairly good, but significant biases are found in some cases, with several models showing values which are consistently higher or lower than the observed AAM (note that LOD cannot be used to infer the time-averaged value of AAM, since its definition includes an arbitrary reference level). The dominance of the seasonal cycle is evident in all data sets, with amplitudes significantly less than the observed value visible for several of the models, while greater amplitudes are obtained for others. On interannual time scales, the large signature of the 1982-83 ENSO is clearly seen in both the AAM and LOD time series. This signal is well-captured by several of the models, but not by others. These broad findings are evident in the following detailed intercomparisons of the decadal mean AAM and AAM fluctuations on seasonal and interannual time scales as given by the AMIP models and by operational NMC analyses.

a. Decadal mean

The global atmosphere's super-rotation is its most striking dynamic, long-term feature. During the AMIP decade 1979-1988, the observed mean value is 1.51×10^{26} kg m^2 s^{-1} which, if transferred to the underlying solid Earth would, if the solid Earth were perfectly rigid, reduce the length of the day by 2.5 ms (see equations (A7), (A9), (A10) and (A11)). Values yielded by each of the AMIP models are plotted in Figure 3, along with the median and IQR of the model values. The model median M^w is

Figure 3 near here

only 3.5% larger than the observed value with 10 of the 23 model values within ± 5% of the observed. More significant departures from the observed value are found in other models, 5 of which give values differing by more than 15% from the observed. Included in this group of poorer results is that from the NMC; because versions of the NMC model were at the heart of the four-dimensional data assimilation system that created the validation values used here, the NMC model's lack of success in Figures 2 and 3 suggests that observations are indeed capable of modifying a model's initial guess field in modern data assimilation schemes.

Figures 2 and 3 suggest that biases in GCM simulations of the zonal wind field are not uniform, and the identification of the causes of the observed discrepancies may not be straightforward. The difficulties involved are evident from Figure 4, in which the

Figure 4 near here

decadal-mean observed $[u]$ and the errors in $[u]$ are shown for those models that yield, respectively, the two largest and the two smallest values of M^w in Figure 3. Remarkably, the meridional distribution of the bias in $[u]$ shows wide variations, even within each class of model errors in M^w. Thus, the main source of the large value for the decadal mean of M^w seen in the UCLA model is excess values of $[u]$ above 200 mb from 60°N to 60°S, whereas the erroneously large NCAR value of M^w arises primarily from $[u]$ errors below 200 mb. The low value of the mean M^w seen in the NMC model results arises from systematically low values of $[u]$ throughout the tropics, particularly in the upper troposphere and lower stratosphere, whereas the very low value of the mean M^w from the DNM results has its source in extratropical regions, with the tropics contributing a positive but smaller bias.

For comparison, Figure 5 gives the $[u]$-bias field for the GLA model, whose

Figure 5 near here

decadal-mean M^w lies closest to that observed for 1979-1988. It appears that success in reproducing the global mean value of M^w need not imply similar success with the decadal-mean $[u]$ field, for the magnitude of the $[u]$ biases evident in Figure 5 is of the same order as those shown in Figure 4 for the outlier M^w simulations. Evidently, for the GLA model at least, the good performance for decadal-mean M^w arises from the cancellation among regional biases in $[u]$ of opposite sign, biases which in many locations are comparable to the observed value of $[u]$ there (cf. Figure 4a). The (area-weighted) mean absolute error in $[u]$ for the GLA field in Figure 5 is 2.3 ms^{-1}. At 1.9 ms^{-1} (IQR = 2.3–1.7 ms^{-1}), typical values of this statistic are smaller than the observed mean absolute value of $[u]$ in Figure 4a, 8.5 ms^{-1}, but not by so much that we can be sanguine about this aspect of the performance of the models.

Despite the differences shown in Figure 4 for $[u]$ among an outlier subset of AMIP models, it remains of interest to quantify the similarity in model biases among the general population of AMIP models. To this end, we have performed an empirical orthogonal function (EOF) analysis of the biases present in the set of $m_b{}^w$ values in the 46 belts for the 23 models. Three significant modes of common variability in the belt momentum error distribution emerge (Figure 6) which together explain more than 87% of

Figure 6 near here

the variance in the full ensemble of $m_b{}^w$ biases. Mode 1, involving errors primarily in northern and southern mid-to-high latitudes with a tendency for smaller, compensating errors in the subtropics, is notable in that the weights for 19 of the models in its principal component are of the same sign. Recognizing that errors for a particular model are often spread across all three modes, the commonality of behavior expressed by mode 1's principal component nevertheless suggests the existence of a shared, underlying difficulty in modeling the climatological, regional distribution of angular momentum. Mode 2 reveals a pattern in which biases in the tropics and in northern midlatitudes are in opposition, and mode 3 emphasizes behavior in southern extratropics.

b. Seasonal cycle

The seasonal cycle in AAM derives from the asymmetry in the land-ocean distributions of the northern and southern hemispheres and the resulting difference in the seasonality of the two hemispheres' subtropical jets [Rosen *et al.*, 1991b]. Because the seasonal cycle represents the largest mode of variability in the AAM time series, it is important that GCMs be able to replicate this signal well. It is encouraging, therefore, to see in Figure 7 that the AMIP models do tend to reproduce the behavior observed in the

Figure 7 near here

climatological monthly mean progression of M^w values. It is worth noting, however, that the models also exhibit a general tendency to underestimate the maximum values observed in December–February. Indeed, in some models this deficiency is quite pronounced, leading to seasonal cycles with distinct maxima around April and November instead of the observed single broad maximum across December through April.

The degree to which the models share common problems in reproducing the observed shape of the seasonal cycle in M^w is revealed by an EOF analysis of the models' composite monthly errors (Figure 8). The tendency of the models to underestimate M^w

Figure 8 near here

during northern winter is apparent in both of the first two modes of this analysis by the preponderance of positive model weights multiplying negative anomalies in the modes' time series then. The first mode in Figure 8 captures errors in the models' estimates of the annual component of M^w, whereas the second mode captures errors in their semiannual component. (The semiannual component of M^w is normally observed to peak in early May, and its amplitude is about 80% of that of the annual component, which peaks in early February; Rosen, 1993). The general shortcoming of the models in December-February appears to project onto a proclivity towards underestimating the annual, while overestimating the semiannual, component of the observed seasonality in M^w.

Figure 9 displays a measure of the amplitude of the seasonal cycle, namely the

Figure 9 near here

standard deviation (σ_S) of the twelve composite calendar-month means of M^w, for each AMIP model and the observed series. The median σ_S value is only some 2.4% larger than the observed σ_S, with nearly half of the model values lying within about 15% of the observed. Nevertheless, notable outliers also exist in Figure 9, so that the range in values for σ_S exceeds a factor of two. There does not appear to be any relationship between errors in a model's seasonal cycle and in its decadal-mean bias, with high values of σ_S being equally likely to be associated with either high or low values of decadal-mean M^w in Figure 3 (and similarly for low values of σ_S). Also shown in Figure 9 is the correlation coefficient (r_s) between each model's series of composite monthly M^w values and the observed series. In conjunction with σ_S, the r_s statistic helps provide a more complete analysis of the fidelity of a model's simulation. Not surprisingly in light of Figure 7, r_s is generally quite large (median = 0.95; IQR = 0.97 - 0.92).

Although the bulk of the observed seasonal variability in $m_b{}^w$ occurs in

Figure 10 near here

connection with the subtropical jets of each hemisphere (Figure 10a), this need not imply that the errors present in Figure 9 originate mostly there. Therefore, to isolate regionally the source of seasonal model errors in M^w, we have calculated for each model: (1) the variance in the difference between the composite monthly mean values of its belt series

$m_b{}^w$ and the observed $m_b{}^w$ values, and (2) the covariance between these seasonal errors in the model belt values and the seasonal errors in global M^w, normalized by the variance in the latter. Because the sum of the covariance in (2) over all 46 belts is equal to the variance in a model's seasonal errors in global M^w, the sum of the 46 values of (2) for a particular model is unity. Hence, (2) provides a convenient measure for quantifying the contribution made by seasonal errors in various regions to the global error, as was done by Rosen *et al.* [1991a] in connection with medium-range forecast model errors.

Errors in the models' simulations of $m_b{}^w$ seasonal cycles are less spatially focused than is the profile of the observed $m_b{}^w$ variance in Figure 10a. Indeed, a plot of (1) as a function of latitude for the 23 models is too noisy to be useful, so Figure 10b attempts to summarize this result by presenting a profile of the median in each belt of all the models' seasonal belt error variances, along with the IQR of these 23 numbers. The large values of the IQR in the figure, especially in the extratropics, attest to the strikingly wide range of model behavior. (Note that the median values plotted in Figure 10 are determined individually for each belt; the profile does not represent the behavior of a single, "median" model.) The largest model errors in simulating the observed seasonal cycles in $m_b{}^w$ tend to flank both sides of the two maxima in Figure 10a, suggesting that errors in positioning the subtropical jets properly are a factor. On the other hand, the amplitude of the largest median errors in Figure 10b is considerably smaller than that of the observed variance peaks in Figure 10a, suggesting that the models do a credible job in reproducing the seasonal change in the *strength* of the subtropical jets.

The fractional covariance between seasonal belt and global momentum errors plotted in Figure 10c indicates that, on average, the model errors that contribute most to failures in reproducing the observed seasonal cycle in M^w originate in the equatormost pair of peaks in Figure 10b, near 20°N and 15°S. The large local errors in northern midlatitudes shown in Figure 10b tend not to be so important for the globally-integrated error. Note again, however, the very large spread in model behavior outside the tropics depicted by the IQR values; for a number of models, errors poleward of the observed positions of the subtropical jets are indeed a major reason for problems with simulating the seasonality in M^w.

c. Interannual variations

The AMIP decade encompassed two ENSO events, those of 1982-1983 and 1986-1987. The former is possibly the strongest such event on record, and the notable positive anomaly in AAM and LOD associated with it led to a resurgence of interest in low-frequency variations in the planetary angular momentum budget. (For recent results and references see Ponte *et al.*, 1994, and Dickey *et al.*, 1994.) The signature of the two ENSO events during 1979-1988 AMIP period is apparent in the observed interannual M^w anomaly series in Figure 11 as a sharp peak in early 1983 and a broader, less intense

Figure 11 near here

maximum from late 1986 through 1987. On average, the AMIP models reproduce the observed interannual anomaly series fairly well, though less successfully than in the case of the seasonal cycle (Figure 7). It is noteworthy that the models, as a group, tend to underestimate the amplitude of the 1982-1983 ENSO signal in AAM but overestimate the 1986-1987 signal. The models also miss the intensity of the negative anomaly observed in 1984, although they do capture the rate of decline in M^w during 1983 fairly well. Notably, though, the models miss even the sign of the anomaly observed during mid-1980 through mid-1981, which according to the NMC observations results mainly from positive wind anomalies in the southern hemisphere tropics (not shown).

Figure 12 gives the interannual standard deviation (σ_I) for each model

Figure 12 near here

separately, along with the correlation coefficient (r_I) between each model's time series of 40 seasonal anomalies and the observed. The median value of σ_I is quite close to the observed, and, as in the case of the seasonal cycle, almost half of the model σ_I values lie within about 15% of the observed, although in the interannual case there is a notable skewness in the distribution toward low values. No relationship between individual σ_I and σ_S values is evident in the data; the performance of each model on one time scale seems to be independent of its performance on the other (see Table 1). A striking

Table 1 near here

difference between overall model performances on seasonal and interannual time scales is that r_I is notably smaller than r_S. The median of r_I is 0.61 with 0.66-0.49 as the corresponding IQR value. On the basis of calculations of the autocorrelation present in the observed and modeled anomaly series, we estimate that in each series the number of degrees of freedom is about 12, implying that a value of r_I greater than about 0.5 is to be regarded as being statistically significant. Sixteen of the models (nearly 70%) exceed this criterion.

Calculations similar to those reported in Figure 10 for the seasonal cycle in $m_b{}^w$ have also been performed for interannual variability in $m_b{}^w$, and these are reproduced in Figure 13. The meridional profile of median model errors in the $m_b{}^w$ interannual

Figure 13 near here

component tends to be spatially correlated with the profile of the observed interannual variance in $m_b{}^w$ (Figure 13a). Unlike the case for the seasonal cycle, local errors in the interannual $m_b{}^w$ component are typically of the same order as the observed signals across the entire profile. Indeed, interannual errors in $m_b{}^w$ are not much smaller than seasonal errors in m_b despite the disparity in the amplitude observed for the two time scales. According to Figure 13b, errors in $m_b{}^w$ within 20° of the equator account for most of the interannual errors in M^w. In light of the relatively small values of IQR also plotted in Figure 13b, this result is rather robust across the suite of 23 AMIP models.

4. DISCUSSION AND SUMMARY OF RESULTS

Here, we have presented results of a study comparing atmospheric angular momentum (AAM) simulations by a variety of AMIP models (Table 1) with the NMC observed values and those inferred from geodetic data. Results from 23 AMIP model runs were considered on three distinct time scales: decadal mean, the seasonal cycle, and interannual variation. Of the 23 models (Table 1), 4 scored well (being within $\pm15\%$ of that observed) on all three time scales, 10 on two out of three, 6 on one of the three and 3 performed poorly on all three time scales. It should be stressed that the GCM results presented here represent "snapshots" (ca. early 1990s) of model evolution that is ongoing at the participating centers. For example, a new gravity-wave drag parameterization scheme has recently been developed at UCLA (Kim and Arakawa 1995), which shows considerable promise for reducing the westerly bias present in the UCLA GCM, in conjunction with an envelope orography (Kim, 1996).

The decadal mean values of AAM were generally well-simulated, with the model median value (1.58×10^{26} kg m^2 s^{-1}) being only 3.5% larger than the observed. Ten of the 23 models produced values that are within 5% of the observed mean; however, 5 of the 23 models are more than 15% away from the observed (Table 1). Examination of the decadal-mean $[u]$ bias with respect to observed winds as a function of latitude and height indicates that contributing errors may be very different in models that show the same characteristic global anomaly (Fig. 4). Furthermore, good agreement with the observed decadal mean cannot be taken to infer similar agreement with the observed $[u]$ fields (Fig. 5), as cancellation among regional differences may combine to produce a low global bias. An EOF analysis performed on angular momentum values in the 46 belts for the 23 models produced 3 dominant modes explaining 87% of the variance. Both Mode 1 (involving errors in the northern and southern mid-to-high latitudes with smaller partially canceling errors in the subtropics) and Mode 2 (bias in the Tropics with compensating bias in the northern midlatitudes) are common to the majority of the models, indicating shared problems in modeling the latitudinal distribution of mean angular momentum.

The seasonal cycle results from asymmetry of the land-ocean distribution of the northern and southern hemispheres, and is generally well-simulated in the AMIP models. The median seasonal standard deviation (σ_s) value is 2.4% larger than observed, with 10 of the models being within 15% of the observed amplitude (Fig. 9 and Table 1). Four of the five models with decadal means that do not lie within 15% of the observed have seasonal variations that do not lie within 15% of the observed value, suggesting that there may be some linkage between poor model performance on decadal means and seasonal time scales. The correlation between observed and model seasonal cycles is quite high, with a median value of $r_s = 0.95$ (IQR = 0.97–0.92). An EOF analysis provides insight into common seasonal errors; the first mode shows a tendency for most models to underestimate the annual cycle, while the second mode largely reflects overestimates of the semi-annual cycle (Fig. 8), both consistent with the models' tendency to underestimate global AAM during northern hemisphere winter. The observed seasonal cycle in AAM is dominated by contributions from the subtropical jets from each hemisphere (Fig. 10), whose strength is generally well reproduced by the models. The largest regional model errors, whose seasonal variance is about an order of magnitude smaller than the observed variance (Fig. 10), tend to border on both sides of the two hemispheric maxima, indicating that errors in positioning the subtropical jets are an issue. Further, examination of the fractional covariance between the regional and global momentum errors (Fig. 10) indicates that most of the seasonal M^w errors originate equatorward of the subtropical jets.

The models' interannual AAM variability is fairly realistic, with the median value of σ_I being quite close to the observed value and ten of the model σ_I values lying within

15% of the observed. Although less robust than the seasonal cycle, the correlation between the observed and model interannual series has a statistically significant median value of 0.61. The two ENSO events during the AMIP decade are clearly evident; however, accurate simulation of intensities of the AAM signatures of individual episodes is generally lacking, as the 1982-1983 event is underestimated and the 1986-87 event is overestimated by the model consensus (Fig. 11). Examination of the latitudinal error covariance structure shows that errors within 20° of the equator account for most of the interannual mismodeling of M^w (Fig. 13b). No relationship is evident between errors on interannual and seasonal time scales in a given model (see Table 1).

The principal objective of AMIP is to identify deficiencies in numerical models so that they can be removed. Except near the equator, the thermal wind relationship based on quasi-geostrophic balance in the horizontal and hydrostatic balance in the vertical relates the vertical rate of change of horizontal wind to the local horizontal gradient of potential density, which depends on temperature, pressure, and moisture content. In using this relationship to obtain a good leading approximation to the wind itself at a general point in the atmosphere, there is a horizontal function of integration which can be evaluated from the surface winds. It follows that any model that satisfactorily represents both (a) surface winds, and (b) horizontal variations of temperature and moisture content should score well on the angular momentum assessment carried out in this paper, and conversely. It is possible, of course, that models that represent angular momentum fluctuations well might, owing to compensating errors, be doing so for the wrong reasons. For example, many of the models participating in the AMIP campaign show cold biases in both the tropics and extratropics [Fiorino, 1995]; the matching sign of these temperature biases serve to minimize errors in the meriodional temperature gradient, which in turn helps many of the models to achieve realistic values for the decadal mean AAM.

In any event, it is obvious that any modeling groups exploiting the results presented in this paper should in the first instance examine those features of the model that determine the pattern of surface winds and the distribution of temperature and moisture within the atmosphere. Of particular importance will be parameterization schemes for representing oceanic and continental boundary layers, mechanical interactions of the atmosphere with orography, including drag due to the excitation of gravity waves, and the role of moist convection and radiative processes in the atmosphere, where the presence of clouds introduces serious complications now being studied intensively in various meteorological research centers.

These remarks might facilitate the use of atmospheric angular momentum "skill scores" in the important and by no means straightforward task of identifying deficiencies in parameterization schemes used in numerical models, with a view to improving the schemes. Much careful work will be needed, however, for a cursory inspection of skill scores reveals no striking correlations with any of the manifold characteristics (see above paragraphs) of the various models used by groups participating in AMIP (cf. Phillips, 1994). In fact, no common characteristics are shared by the four models that are successful on all three time scales. The continuing Atmospheric Model Intercomparison Project will provide opportunities to pursue the necessary investigations.

Acknowledgments. We thank the members of the modeling groups who sent results to the Atmospheric Model Intercomparison Project (AMIP) of the World Climate Research Programme (WCRP) and we especially wish to thank W. L. Gates and his colleagues at the Lawrence Livermore Laboratory, who coordinated the AMIP effort. We acknowledge interesting discussions with C. R. Mechoso, K. Sperber, and G. H. White. The work of J. O. Dickey and S. L. Marcus was carried out at the Jet Propulsion Laboratory, California Institute of Technology, under contract with the National Aeronautics and Space Administration. Programming assistance at AER was provided by P. Nelson. The work of R. D. Rosen and D. A. Salstein was supported in part by the National Science

Foundation Climate Dynamics Program under grant ATM-9223164, and NASA's Mission to Planet Earth Program under Contract NAS5-32861 and Grant NAGW-2615.

APPENDIX A: ATMOSPHERIC EXCITATION OF EARTH'S ROTATION VARIATIONS

The absolute angular momentum of the atmosphere, a three-dimensional vector $M_i = M_i(t)$ (where t denotes time), can be written as the sum of two terms

$$M_i \equiv M_i^P + M_i^W \tag{A1}$$

where
$$M_i^P \equiv \iiint \rho \varepsilon_{ijk} x_j \varepsilon_{klm} \omega_l x_m d\tau \tag{A2a}$$

and
$$M_i^W \equiv \iiint \rho \varepsilon_{ijk} x_j u_k d\tau, \tag{A2b}$$

respectively the 'matter' (or pressure) and the 'wind' contributions to M_i. Here $\rho(x_i,t)$ and $u_k(x_i,t)$ denote the mass density and wind velocity respectively at a general point, $x_i, i = 1,2,3$ within the atmosphere, and $d\tau$ is a volume element of the atmosphere, over the whole of which the volume integral is taken. The usual summation convention is used for repeated suffixes, and ε_{ijk} is the alternating tensor with values 0 or $\pm$ 1. The frame of reference used has its origin at the center of mass of the whole Earth (solid inner core, liquid outer core, 'solid Earth', hydrosphere, atmosphere) and is aligned with the principal axes of inertia of the 'solid Earth' (mantle, crust and cryosphere). With respect to an inertial frame, the rotation of the solid Earth has angular velocity $\omega_i(t)$, $i = 1, 2, 3$.

All components of M_i vary with time as a consequence of dynamical interactions between the atmosphere and the underlying planet, which produce measurable fluctuations in ω_i. It is customary to write

$$\omega_i(t) \equiv (\omega_1(t), \omega_2(t), \omega_3(t)) \equiv \Omega(m_1(t), m_2(t), 1 + m_3(t)), \tag{A3}$$

where Ω = 7.292115 x 10^{-5} radians per second is the mean angular speed of sidereal rotation of the solid Earth in recent times. Over time scales that are short compared with those of geological processes, the magnitudes of the dimensionless quantities $m_1(t)$, $m_2(t)$ and $m_3(t)$ are all very much less than unity, so that for the purpose of determining M_i from meteorological data using equations (A2), it is sufficient to set $m_i = 0$, so that $\omega_i =$ (0, 0, Ω).

The non-zero meteorological contributions to $m_i(t)$ are, of course, important in the study of fluctuations in the Earth's rotation. If L_i (i = 1, 2, 3), is the net torque acting on the Earth's atmosphere then

$$L_i = dM_i / dt = \dot{M}_i + \varepsilon_{ijk}\omega_j M_k, \tag{A4}$$

where dM_i/dt and $\dot{M}_i$ are the time rates of change M_i in an inertial frame and in the rotating frame respectively. When $\omega_i = (0, 0, \Omega)$ we have

$$L_1 = \dot{M}_1 - \Omega M_2, L_2 = \dot{M}_2 - \Omega M_2, L_3 = \dot{M}_3 \tag{A5}$$

It is well known that L_i cannot be determined as accurately as M_i from surface drag and pressure force determinations, owing to limited measurements, parameterization difficulties, and the high degree of cancellation involved. But it can be determined indirectly with useful accuracy from mass and wind observations at all levels within the atmosphere by using the expressions given by equations (A4) [White, 1991 and 1993; Salstein and Rosen, 1994]. Through the action of L_i, angular momentum is exchanged back and forth between the atmosphere and the underlying planet, the surface of which is subjected by the atmosphere to an applied torque equal to $-L_i$. Most of the angular momentum exchanged, which in magnitude can be a considerable fraction of that of M_i^w, goes into the massive solid Earth, whose moment of inertia is some 10^6 times that of the atmosphere. This produces (a) tiny but measurable changes in the length of the day

$$\Lambda(t) = \Lambda_0 / (1 + m_3(t)), \ \textit{where}\ \Lambda_o \equiv 2\pi / \Omega, \tag{A6a}$$

as well as (b) movements of the poles of the instantaneous axis of rotation of the solid Earth relative to its axis of figure, as specified by the quantity

$$m(t) \equiv m_1(t) + \mathrm{i}\, m_2(t) \tag{A6b}$$

where $\mathrm{i} \equiv \sqrt{-1}$). See equation (A3). Indeed, the strongest torques acting on the solid Earth are generated by atmospheric motions, which produce easily detectable changes in Λ of up to about 1 ms in magnitude (corresponding to change in $|m_3|$ of about 10^{-8}) and displacements of the pole of rotation of several metres (corresponding to changes in $|m|$ of about 10^{-6}).

The torque $-L_i$ produced by atmospheric motions on the underlying planet is due to (a) tangential stresses in the turbulent boundary layers over the continents and oceans, and (b) normal stresses acting on orography and the Earth's equatorial bulge. Owing to the rigidity (albeit slightly imperfect) of the solid Earth, all three components of the 'continental' part of $-L_i$ are transmitted to the solid Earth directly and fully. The oceanic part of $-L_i$ gives rise to a dynamical response in the oceans which requires further investigation, but the case when the whole of the applied torque is assumed to be passed on by the oceans to the solid Earth virtually instantaneously can be taken as realistic for most practical purposes, particularly when dealing with the axial component of $-L_i$ and the changes in Λ that it produces [Ponte, 1990]. Thus, the oceans act as an intermediary in the angular momentum exchange process, by transmitting the applied stresses in the atmospheric boundary layer over the oceans to the continental margins and ocean bottom. It is a convenient circumstance that, owing to the slowness and scales of ocean currents in comparison with atmospheric winds, in the budget of angular momentum between the solid Earth and its overlying fluid layers, the hydrosphere (in spite of its much greater moment of inertia than that of the atmosphere, by a factor of about 300) produces effects which can be neglected to a first approximation.

In the theory of the interactions between the atmosphere and underlying planet that give rise to fluctuations in M_i, the analysis is facilitated by using in place of M_i the dimensionless AAM functions χ_i, i = 1, 2, 3, (see Barnes *et al.*, *1983*). They can be defined as follows:

$$\chi_i \equiv \chi_i^P + \chi_i^w = \int_{-\pi/2}^{\pi/2} \xi_i(\phi,t)\; d\phi = \int_{-\pi/2}^{\pi/2} \left[\xi_i^P(\phi,t) + \xi_i^w(\phi,t)\right] d\phi, \tag{A7}$$

where

$$(\xi_1^P, \xi_2^P) \equiv \frac{-1.098 R^4}{g(C-A)} \int_0^{2\pi} p_s \cos^2\phi \sin\phi\,(\cos\lambda, \sin\lambda)\, d\lambda, \tag{A8a}$$

$$(\xi_1^w, \xi_2^w) \equiv$$

$$\frac{-1.5913 R^3}{g(C\text{-}A)\Omega} \int_0^{P}\int_0^{2\pi} \cos\phi \left\{ u \sin\phi\,(\cos\lambda, \sin\lambda) - v\,(\sin\lambda, -\cos\lambda) \right\} d\lambda dp, \tag{A8b}$$

and

$$(\xi_3^P, \xi_3^w) = \left(\frac{0.753 R^4}{g C_m} \int_0^{2\pi} p_s \cos^3\phi \;\; d\lambda, \frac{0.998 R^3}{g C_m \Omega} \int_0^{P}\int_0^{2\pi} u \cos^2\phi \, d\lambda \, dp \right). \tag{A9}$$

In these expressions, (ϕ, λ) denote latitude and longitude respectively, $p_s(\phi, \lambda, t)$ is the surface pressure and $u\,(\phi, \lambda, p, t)$ and $v\,(\phi, \lambda, p, t)$ are the eastward and northward components respectively of the wind velocity at pressure level p. We take R = 6.3674 x 10^6 m for the mean radius of the solid Earth, Ω = 7.292115 x 10^{-5} rad s^{-1} for its mean rotation rate, g = 9.810 m s^{-2} for the mean acceleration due to gravity, C = 8.0376 x 10^{37}

kg m^2 for the polar moment of inertia of the whole Earth, $(C-A) = 2.610 \times 10^{35}$ kg m^2 where A is the corresponding equatorial moment of inertia, and $C_m = 7.1236 \times 10^{37}$ kg m^2 is the polar moment of inertia of the Earth's mantle and crust. The coefficients 1.098, 1.5913, 0.753, and 0.998 incorporate the so-called 'Love number' corrections, which allow for concomitant meteorologically-induced tiny but dynamically significant changes in the inertia tensor of the slightly deformable solid Earth, using the most up-to-date geophysical data (see Eubanks, 1993). The dimensionless pseudo-vector χ_i is related to the AAM vector M_i, with the equatorial components (χ_1, χ_2) and (M_1, M_2) scaled differently from the axial components χ_3 and M_3. Routine determinations of χ_i have been made for several years at several meteorological centers (using older values of the "Love number" corrections, namely 1.00, 1.43, 0.70 and 1.00 respectively in place of 1.098, 1.5913, 0.753 and 0.998, C_m in place of C and A_m in place of A in equations (A8)).

Any change in M_3 is accompanied by an equal and opposite change in the axial component of the angular momentum of the solid Earth (since the fluctuations in the azimuthal motion of the underlying liquid core of moment of inertia ~$0.1C$ are effectively decoupled from those of the solid Earth on the short time scales with which we are concerned here). In terms of the dimensionless quantities m_3 and χ_3 this can be expressed as

$$\dot{m}_3 + \dot{\chi}_3 = 0 \tag{A10}$$

with solution

$$m_3(t) + \chi_3(t) = m_3(t_0) + \chi_3(t_0), \tag{A11}$$

where $m_3(t_0)$ and $\chi_3(t_0)$ are constants of integration equal respectively to m_3 and χ_3 at some initial instant $t = t_0$. The dominant contribution to fluctuations in χ_3 comes from the 'wind' term χ_3^w, which depends on the distribution in the meridional plane of the average with respect to longitude λ of the eastward (westerly) wind speed. If one considers only the wind contribution, equation (A7) for the axial component simplifies to

$$\chi_3^w = \frac{0.998(2\pi)\overline{R}^3}{gC_m\Omega} \int_0^{P_s} \int_{-\pi/2}^{\pi/2} [u] \cos^2 \phi \, d\phi \, dp. \qquad \text{(A12)}$$

in which case M_3, the axial atmospheric angular momentum, reduces to

$$M_3^w = 2\pi g^{-1} \overline{R}^3 \int_0^{P_s} \int_{-\pi/2}^{\pi/2} [u] \cos^2 \phi \, d\phi \, dp. \qquad \text{(A13)}$$

REFERENCES

Anderson, J. D., and R. D. Rosen, The latitude-height structure of 40-50 day variations in atmospheric angular momentum, *J. Atmos. Sci.*, *40*, 1584-1591, 1983.

Barnes, R. T. H., R. Hide, A. A. White, and C. A. Wilson. Atmospheric angular momentum fluctuations, length of day changes and polar motion, *Proc. R. Soc. Lon.*, *A387*, 31-73, 1983.

Bell, M. J., R. Hide, and G. Sakellarides, Atmospheric angular momentum forecasts as novel tests of global numerical prediction models, *Phil. Trans R.Soc. Lon.*, *A334*, 55-92, 1991.

Boer, G., Earth-atmosphere exchange of angular momentum simulated in a general circulation model and implications for the length-of-the-day, *J. Geophys. Res.*, *95*, 5511-5531, 1990.

Chao, B. F., Interannual length of day variations with relation to the Southern Oscillation/El Niño, *Geophys. Res. Letts.*, *11*, 541-544, 1984.

Chao, B. F., Correlation of interannual lengths-of-day variation with El Niño/Southern Oscillation, 1972-1986, *J. Geophys. Res.*, *93*, B7, 7709-7715, 1988.

Chao, B. F., Length-of-day variations caused by El Niño/Southern Oscillation and the Quasi-Biennial Oscillation, *Science*, *243*, 923-925, 1989.

Dickey, J. O., Atmospheric excitation of the earth's rotation: Progress and prospects via space geodesy, in *Contributions of Space Geodesy to Geodynamics, Earth Dynamics*, edited by D. E. Smith and D. L. Turcotte, *Am. Geophys. Un.*, Washington, D.C., 55-70, 1993.

Dickey, J. O., M. Ghil, and S. L. Marcus, Extratropical aspects of the 40-50 day oscillation in length of day and atmospheric angular momentum, *J. of Geophys. Res.* *96*, 22,643-22,658, 1991.

Dickey, J. O., S. L. Marcus, and R. Hide, Global propagation of interannual fluctuations in atmospheric angular momentum, *Nature*, *357*, 484-488, 1992.

Dickey, J. O., S. L. Marcus, T. M. Eubanks, and R. Hide, Climate studies via space geodesy: Relationships between ENSO and interannual length-of-day variations, in *Interactions Between Global Climate Subsystems: The Legacy of Hann, Geophys. Monogr. Ser.*, vol. 75, edited by G. A. McBean and M. Hantel, pp. 141-155, AGU, Washington, D.C., 1993a.

Dickey, J. O., S. L. Marcus, C. M. Johns, R. Hide, S. R. Thompson, The oceanic contribution to the earth's seasonal angular momentum budget, *Geophys. Res. Lett.*, *20*, 2953-2956, 1993.

Dickey, J.O., S.L. Marcus, R. Hide, T.M. Eubanks, and D.H. Boggs, Angular momentum exchange among the solid earth, atmosphere, and oceans: A case study of the 1982-1983 El Niño event, *J. Geophys. Res.*, *99*, 23,921-23,937, 1994.

Eubanks, T. M., Variations in the orientation of the Earth, in *Contribution of Space Geodesy and Geodynamics: Earth Dynamics. Geodyn. Ser., vol. 24*, edited by D. E. Smith and D. L. Turcotte, pp. 1-54, American Geophysical Union Monograph. Washington D. C., 1993.

Eubanks, T. M., J. A. Steppe, and J. O. Dickey, The El Niño, the Southern Oscillation and the Earth's Rotation, in *Earth Rotation; Solved and Unsolved Problems, NATO Advanced Institute Series C: Mathematical and Physical Sciences, 187*, ed. A. Cazenave, 163-186, D. Reidel, Hingham, Mass., 1986.

Fiorino, M., AMIP Overview—An Analysis of the Base State, in *Proceedings of the First International AMIP Scientific Conference*, 15-19 May, 1995, Monterey, CA, WCRP-92, WMO/TD-No. *732*, 531, 1995.

Gates, W.L., AMIP: The Atmospheric Model Intercomparison Project, *Bull. Amer. Meteor. Soc.*, *73*, 1962-1970, 1992.

Hide, R., N. T. Birch, L. V. Morrison, D. J. Shea, and A. A. White, Atmospheric angular momentum fluctuations and changes in the length of the day, *Nature*, *286*, 114-117, 1980.

Hide, R. and J. O. Dickey, Earth's variable rotation, *Science*, *253*, 629-637, 1991.

Jordi, C., L. V. Morrison, R. D. Rosen, D. A. Salstein, and G. Rossello, Fluctuations in the earth's rotation since 1830 from high resolution astronomical data, *Geophys. J. Int.*, *117*, 811-818, 1994.

Kim, Y.-J., Representation of subgrid-scale orographic effects in a general circulation model: Impact on the dynamics of simulated January climate, *J. Clim*, submitted. 1996.

Kim, Y.-J., and A. Arakawa, Improvement of orographic gravity-wave parameterization using a mesoscale gravity-wave model, *J. Atmos. Sci., 52,* 1875-1902, 1995.

Lanzante, J.R., Resistant, robust and nonparametric techniques for the analysis of climate data: Theory and examples, including applications to historical radiosonde station data, submitted manuscript, 1996.

Marcus, S. L., M. Ghil, and J. O. Dickey, The Extratropical 40-day oscillation in the UCLA general circulation model, Part I: Atmospheric angular momentum, *J. Atmos. Sci., 51*, 1431-1466, 1994.

Marcus, S. L., M. Ghil, and J. O. Dickey, The Extratropical 40-day oscillation in the UCLA general circulation model, Part II: Spatial structure, *J. Atmos. Sci.*, accepted, 1995.

Marcus, S. L., and J. O. Dickey, Coupled poleward propagation of sea surface temperature and atmospheric angular momentum anomalies: Results from AMIP, *Sixth Conference on Climate Variations*, American Meteorological Society, 70-74, 1994a.

Phillips, T. J., *A Summary Documentation of the AMIP Models*, PCMDI Report No. 18, Program for Climate Model Diagnosis and Intercomparison, Lawrence Livermore National Laboratory, Livermore, CA, 343 pp, 1994.

Ponte, R. M., Barotropic motions and the exchange of angular momentum between the oceans and solid earth, *J. Geophys. Res.*, *95*, 11,369-11, 374, 1990.

Ponte, R. M., R. D. Rosen, and G. J. Boer, Angular momentum and torques in a simulation of the atmosphere's response to the 1982-83 El Niño, *J. Climate*, *7*, 538-550, 1994.

Rosen, R.D., The axial momentum balance of earth and its fluid envelope, *Geophys.*, *14*, 1-29, 1993.

Rosen, R. D. and D. A. Salstein, Contribution of stratospheric winds to annual and semi-annual fluctuations in atmospheric angular momentum and the length of day, *J. Geophys. Res.*, *90*, 8033-8041, 1985.

Rosen, R.D., and D.A. Salstein, Variations in atmospheric angular momentum on global and regional scales and the length of day, *J. Geophys. Res.*, *88*, 5451-5470, 1983.

Rosen, R. D., D. A. Salstein, T. M. Eubanks, J. O. Dickey, and J. A. Steppe, An El Niño signal in atmospheric angular momentum and earth rotation, *Science*, *225*, 411-414, 1984.

Rosen, R.D., D.A. Salstein, and T. Nehrkorn, Predictions of zonal wind and angular momentum by the NMC Medium-Range Forecast Model during 1985-89, *Mon. Wea. Rev.*, *119*, 208-217, 1991a.

Rosen, R. D., D. A. Salstein, and T. M. Wood, Zonal contributions to global momentum variations on intraseasonal through interannual time scales, *J. Geophys. Res.*, *96*, 5145-5151, 1991b.

Rosen, R. D., D. A. Salstein, and T. M. Wood, Discrepancies in the earth-atmosphere angular momentum budget, *J. Geophys. Res.*, *95*, 265-279, 1990.

Rosen, R.D., D.A. Salstein, A. J. Miller, and K. Arpe, Accuracy of atmospheric angular momentum estimates from operational analyses, *Mon. Wea. Rev.*, *115*, 1627-1639, 1987.

Salstein, D. A., and R. D. Rosen, Topographic forcing of the atmosphere and a rapid change in the length-of-day, *Science*, *264*, 407-409, 1994.

Salstein, D. A., and R. D. Rosen, Earth rotation as a proxy for interannual variability in atmospheric circulation, 1860-present, *J. Clim. Appl. Meteorol.*, *25*, 1870-1877, 1986.

Salstein, D. A., D. M. Kann, A. J. Miller, and R. D. Rosen, The Sub-Bureau for Atmospheric Angular Momentum of the International Earth Rotation Service (IERS): A meteorological data center with geodetic applications, *Bull. Am. Met. Soc.* *74*, 67-80, 1993.

White, G. H., in "Proceedings of the American Geophysical Union Chapman Conference on Geodetic VLBI: Monitoring Global Change," *Nat. Oceanic Atmos. Adm. Tech. Rep. NOS 137 NGS 49*, 262, 1991.

White, G. H., in "Research Activities in Atmospheric and Oceanic Modeling," *CAS/JSC Work Group Numer. Exp. Rep. no. 18* (World Meteorological Organization, Geneva, 2.3-2.4, 1993.

LEGENDS FOR FIGURES

Figure 1. Time series of irregular fluctuations in the length of the day (LOD) from 1963 to 1992 (curve a) and its decadal, interannual, seasonal, and intraseasonal components (curves b, c, d and e, respectively). The decadal (curve b) component largely reflects angular momentum exchange between the solid Earth and the underlying liquid metallic outer core produced by torques acting at the core-mantle boundary. The other components (curves c, d and e) largely reflect angular momentum exchange between the atmosphere and the solid Earth, produced by torques (proportional to the time-derivative of the LOD time series) acting directly on the solid Earth over continental regions of the Earth's surface and indirectly over oceanic regions (adapted from Hide and Dickey, 1991).

Figure 2. The axial component of atmospheric angular momentum (M^W), determined from the monthly standard output for 23 AMIP models which extends up to the 50 mb level (solid lines). The dashed and dotted lines (repeated in each panel) show respectively M^W determined from the operational NMC analysis for the AMIP decade, and global angular momentum fluctuations inferred from geodetic data (a quadratic offset has been removed from the geodetic LOD determinations to account for core-mantle effects). 1 emsu (equivalent millisecond unit) of axial angular moment corresponds to 0.67×10^{26} kg m^2 s^{-1}.

Figure 3. Mean value of the relative angular momentum of the atmosphere between 1000 and 50 mb during the decade 1979-88 for each of 23 models. At the right are plotted the median and the upper and lower quartiles of the distribution of model values, with the length of the vertical line connecting the last two depicting the interquartile range. The

dashed line indicates the value observed for the same decade based on NMC operational analyses.

Figure 4a. Meridional cross section of the average value of the zonal-mean zonal wind observed during the decade 1979-88 based on NMC operational analyses. Standard pressure levels marked along the ordinate correspond to the vertical distribution of the archived analyses. Shaded values are negative (easterlies). The global-mean value of the $[u]$ field shown here is 6.8 ms^{-1}.

Figure 4b. Meridional cross sections of the average value of the zonal-mean zonal wind during the decade 1979-88 for four selected models minus the observed value from Figure 4a. In the left column are the models with the two largest values of M^w in Figure 3; the right column contains the models with the two smallest values of M^w in Figure 3. Negative values are shaded.

Figure 5. Meridional cross section of the average value of the zonal-mean zonal wind during the decade 1979-88 for the GLA model minus the observed value from Figure 4a. Negative values are shaded.

Figure 6. The three leading empirical orthogonal functions (EOFs) of the covariance matrix formed from the 23 model time series of the difference between the decadal-mean model value of the relative angular momentum in each of 46 equal-area belts (m_b^w) and the observed value. The eigenvector on the left is plotted in units of 10^{24} kg m^2 s^{-1}. The weight contributed by each model to each of the EOFs is given on the right in nondimensional, normalized units; the models are shown in the same sequence as in Figure 3. The percent of the variance in all the model's belt momentum biases explained by each EOF is also shown.

Figure 7. The median among the 23 model values of the relative angular momentum of the atmosphere between 1000 and 50 mb for each composite calendar month of 1979-88 (solid line), along with the upper and lower quartiles of the distribution of model values for each composite month. The dashed line indicates the observed composite monthly values, based on NMC operational analyses. The decadal mean of the series for each model and for the observations has been removed prior to generating these results.

Figure 8. The first two empirical orthogonal functions of the covariance matrix formed from the 23 models' time series of their composite monthly values of M^w minus the observed value. The eigenvector on the left is plotted in units of 10^{24} kg m^2s^{-1}. The weight contributed by each model to each of the modes is given on the right in nondimensional, normalized units; the models are shown in the same sequence as in Figure 3. The percent of the variance in all the models' seasonal errors explained by each mode is also shown.

Figure 9. At bottom, the standard deviation of the twelve composite calendar-month means during 1979-88 of the relative angular momentum of the atmosphere between 1000 and 50 mb (M^w) for each of 23 models. To the right on the same scale are plotted the median and the upper and lower quartiles of the distribution of model values. The dashed line indicates the value observed for the same decade based on NMC operational analyses. At top, the correlation coefficient (scale on right) between each model's series of composite monthly M^w values and the observed series.

Figure 10(a). The variance observed in the composite calendar-month values of the relative angular momentum in each of 46 equal-area belts ($m_b{}^w$), based on NMC operational analyses for 1979-1988. (b). The median among the 23 model values of the variance in the difference between a model's composite monthly mean series of $m_b{}^w$ and the observed $m_b{}^w$ series, along with the upper and lower quartiles of the distribution of the 23 model values of this error variance for each belt. (c). The median among the 23 model values of the covariance between the seasonal errors in a model's series of $m_b{}^w$ (i.e., the difference between its composite monthly mean series of $m_b{}^w$ and the observed $m_b{}^w$ series) and the seasonal errors in its series of M^w (i.e., the difference between the model's composite monthly mean series of M^w and the observed M^w series), divided by the variance in the difference between the model's composite monthly mean series of M^w and the observed M^w series. Also plotted are the upper and lower quartiles of the distribution of the 23 model values of this fractional error covariance for each belt.

Figure 11. As in Figure 7, but for the interannual component of the relative angular momentum of the atmosphere between 1000 and 50 mb (M^w) formed by averaging monthly values of M^w in each of 40 seasons during 1979-1988 and subtracting from this series the decadal mean seasonal cycle.

Figure 12. As in Figure 9, but for the interannual component of the relative angular momentum of the atmosphere between 1000 and 50 mb (M^w) formed by averaging monthly values of M^w in each of 40 seasons during 1979-1988 and subtracting from this series the decadal mean seasonal cycle.

Figure 13. (a) As in Figure 10 a and b, but for the interannual component of the relative angular momentum in each of 46 equal-area belts ($m_b{}^w$) formed by averaging monthly values of $m_b{}^w$ in each of 40 seasons during 1979-1988 and subtracting from this series the decadal mean seasonal cycle. (b) As in Figure 10c, but for the interannual component.

Table 1

List of AMIP Models intercompared in this study together with an indication of their performance*

		Decadal Mean	Seasonal σ_s	Interannual σ_I
BMRC	Bureau of Meteorology Research Centre (Australia)	√	√	√
CCC	Canadian Centre for Climate Research	√	√	√
CNRM	Centre National de Recherches Météorologiques (France)	—	√	√
CSIRO	Commonwealth Scientific and Industrial Research Organization (Australia)	√	√	—
DERF	Dynamical Extended-Range Forecasting (at GFDL)	√	√	+
DNM	Department of Numerical Mathematics (of the Russian Academy of Sciences)	—	+	—
ECMWF	European Centre for Medium-Range Weather Forecasts	√	—	√
GFDL	Geophysical Fluid Dynamics Laboratory	√	+	√
GLA	Goddard Laboratory for Atmospheres, NASA	√	√	√
GSFC	Goddard Space Flight Center, NASA	√	√	—
JMA	Japan Meteorological Agency	√	+	√
MGO	Main Geophysical Observatory, Russia	√	+	√
MPI	Max-Planck-Institut für Meteorologie, Germany	√	—	+
MRI	Meteorological Research Institute, Japan	√	√	—
NCAR	National Center for Atmospheric Research	+	+	—
NMC	National Meteorological Center (now NCEP)	—	—	√
NRL	Naval Research Laboratory, Monterey	√	—	+
RPN	Recherche en Prévision Numérique, Canada	√	—	—
SNG	State University of New York at Albany/NCAR	√	+	—
SUNYA	State University of New York at Albany	√	√	—
UCLA	University of California at Los Angeles	+	—	—
UGAMP	The UK Universities' Global Atmospheric Modelling Programme	√	√	√
UKMO	United Kingdom Meteorological Office	√	+	+

* See the three columns on the right, where √ indicates that the model gives a value within 15% of that observed, — a value more than 15% lower than observed and + more than 15% higher.

Figure 1

COMPONENT OF (t)

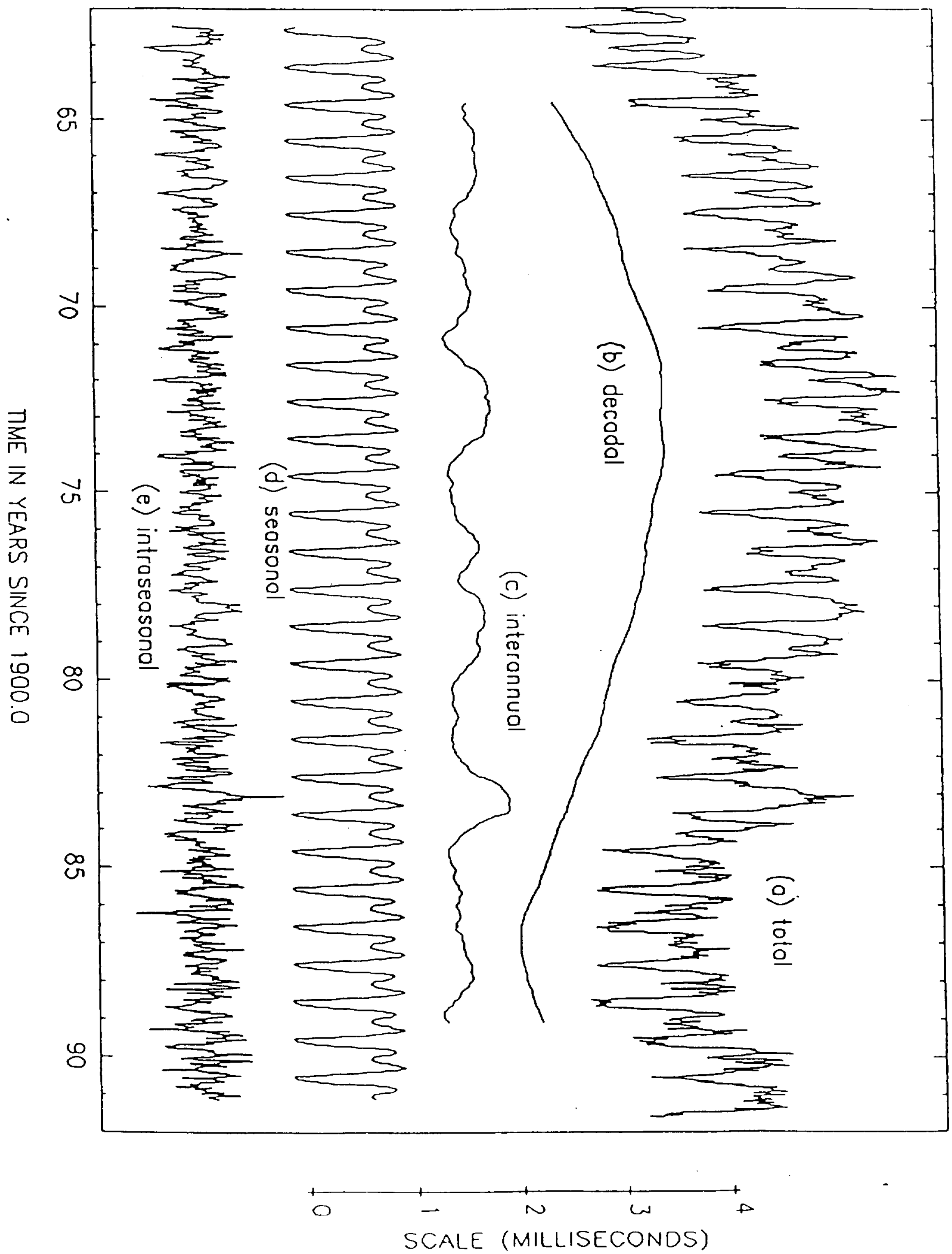

Figure 2

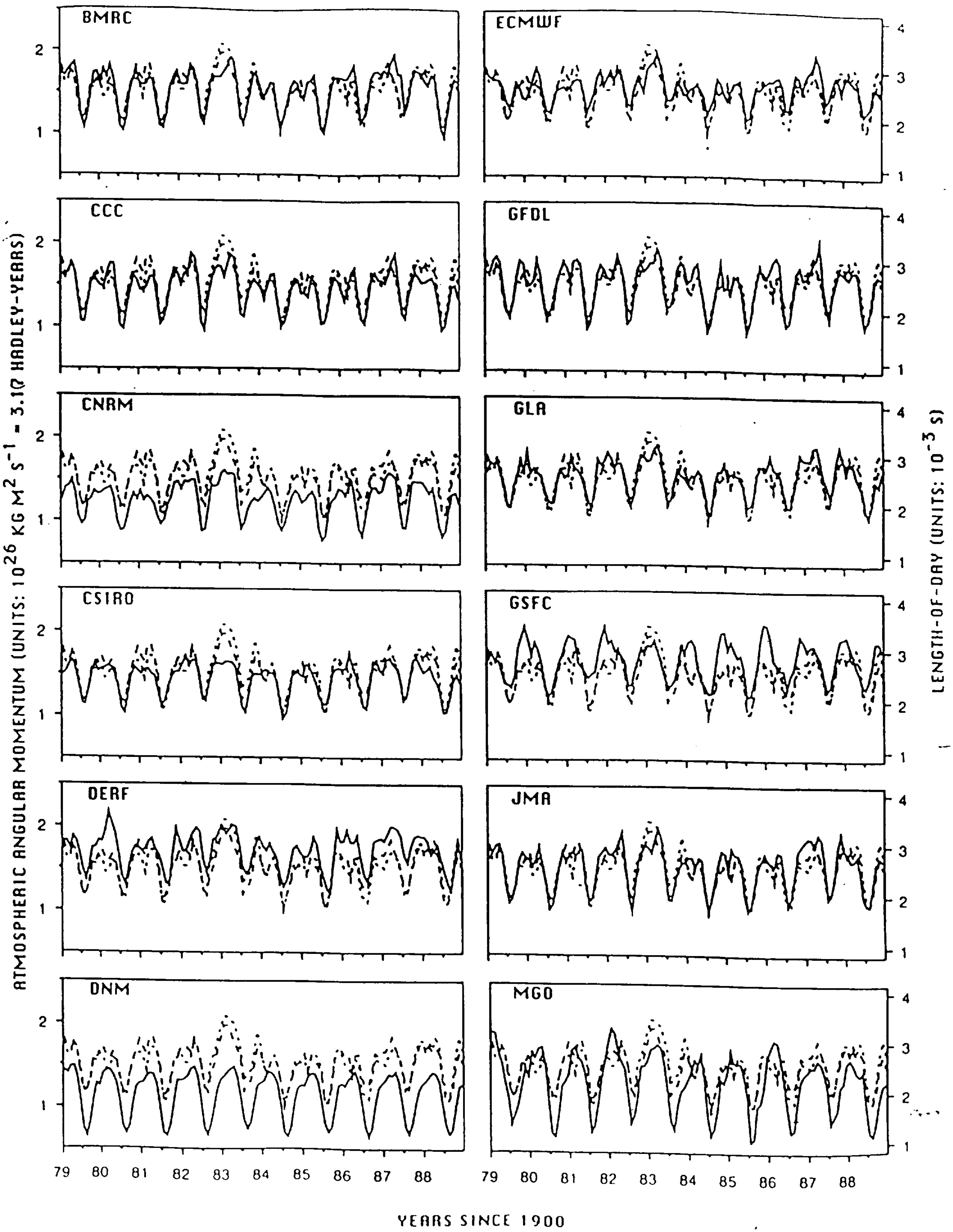

BMRC
ECMWF
CCC
GFDL
CNRM
GLA
CSIRO
GSFC
DERF
JMA
DNM
MGO
ATMOSPHERIC ANGULAR MOMENTUM (UNITS: 10^{26} KG M^2 S^{-1} = 3.17 HADLEY-YEARS)
LENGTH-OF-DAY (UNITS: 10^{-3} S)
79 80 81 82 83 84 85 86 87 88
YEARS SINCE 1900

Figure 2 cont.

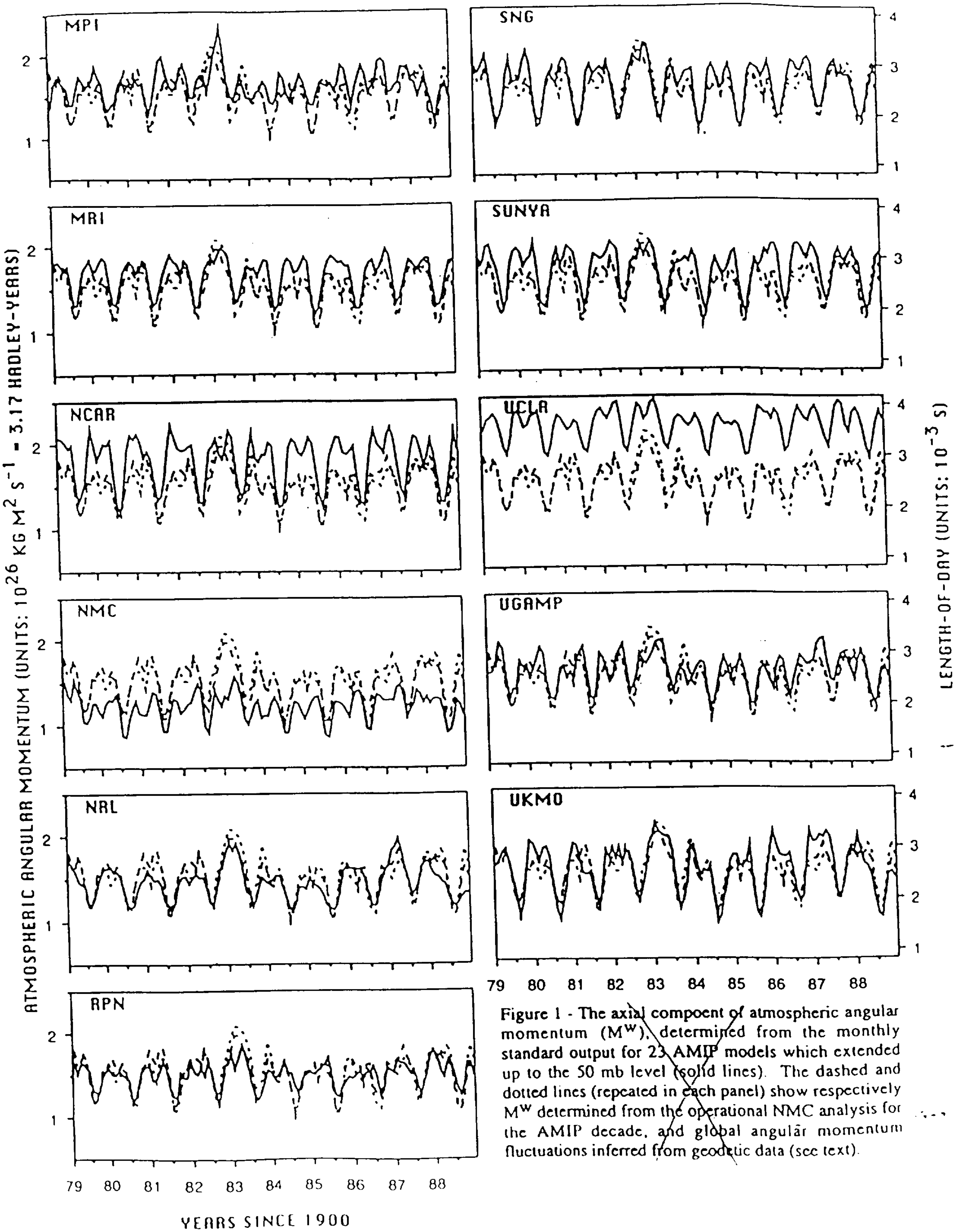

Figure 1 - The axial compoent of atmospheric angular momentum (M^W), determined from the monthly standard output for 23 AMIP models which extended up to the 50 mb level (solid lines). The dashed and dotted lines (repeated in each panel) show respectively M^W determined from the operational NMC analysis for the AMIP decade, and global angular momentum fluctuations inferred from geodetic data (see text).

Figure 3

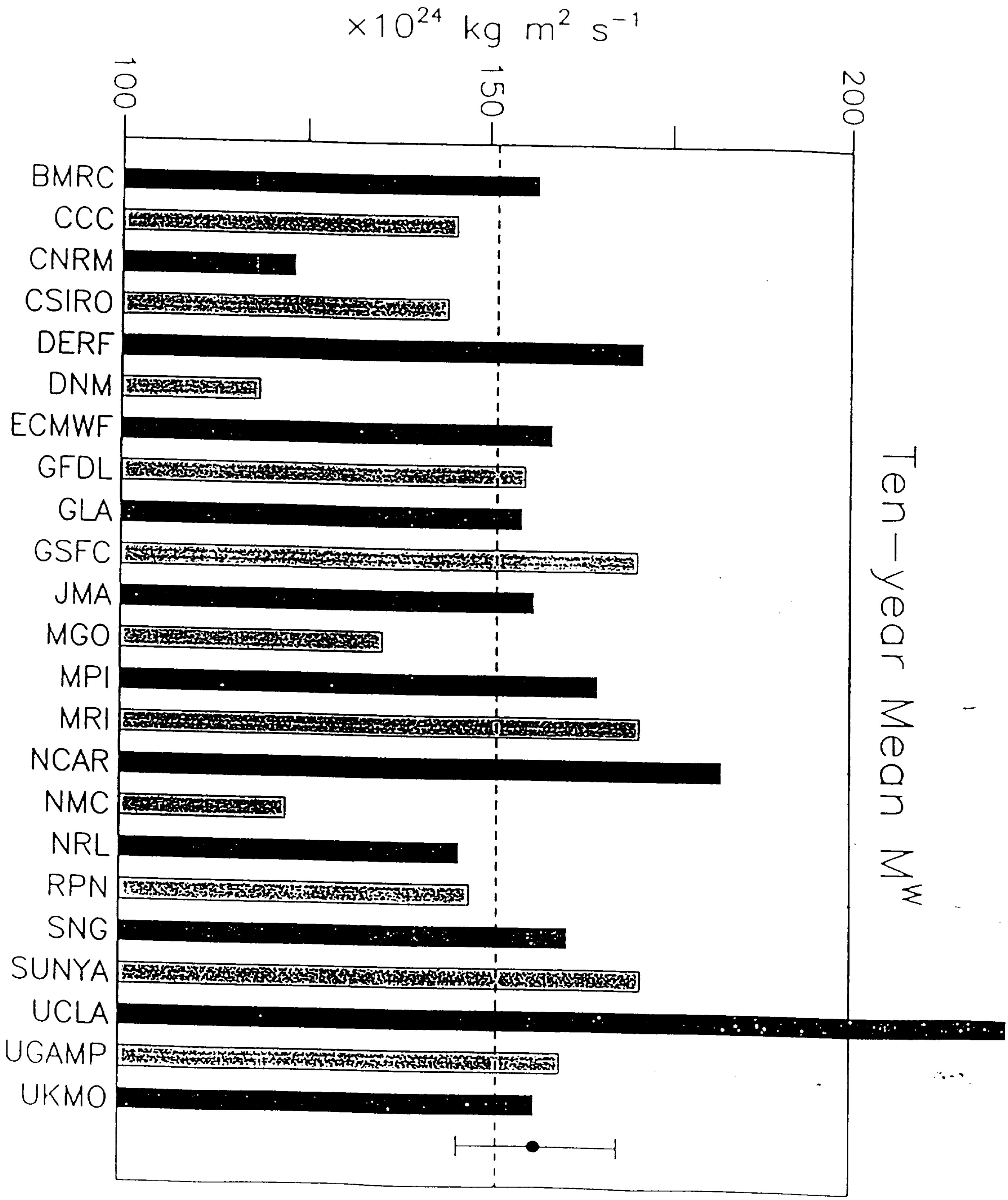
×10^24 kg m^2 s^-1
100
150
200
BMRC
CCC
CNRM
CSIRO
DERF
DNM
ECMWF
GFDL
GLA
GSFC
JMA
MGO
MPI
MRI
NCAR
NMC
NRL
RPN
SNG
SUNYA
UCLA
UGAMP
UKMO
Ten-year Mean M^W

Figure 4a

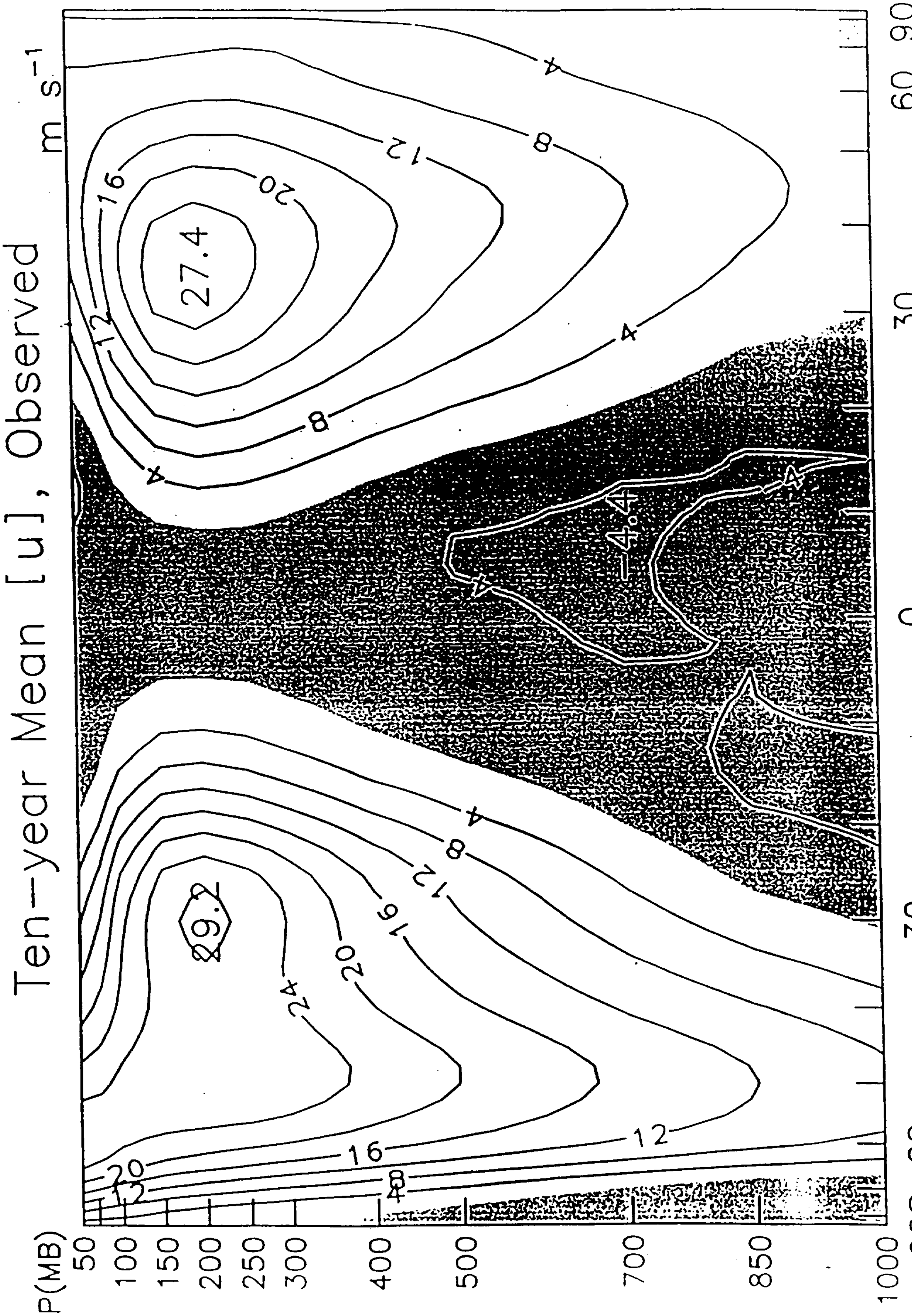

Ten-year Mean [u], Observed m s-1
P(MB)
50
100
150
200
250
300
400
500
700
850
1000
90S
60
30
0
30
60
90N
27.4
29.2
-4.4
24
20
16
12
8
4

Figure 4b

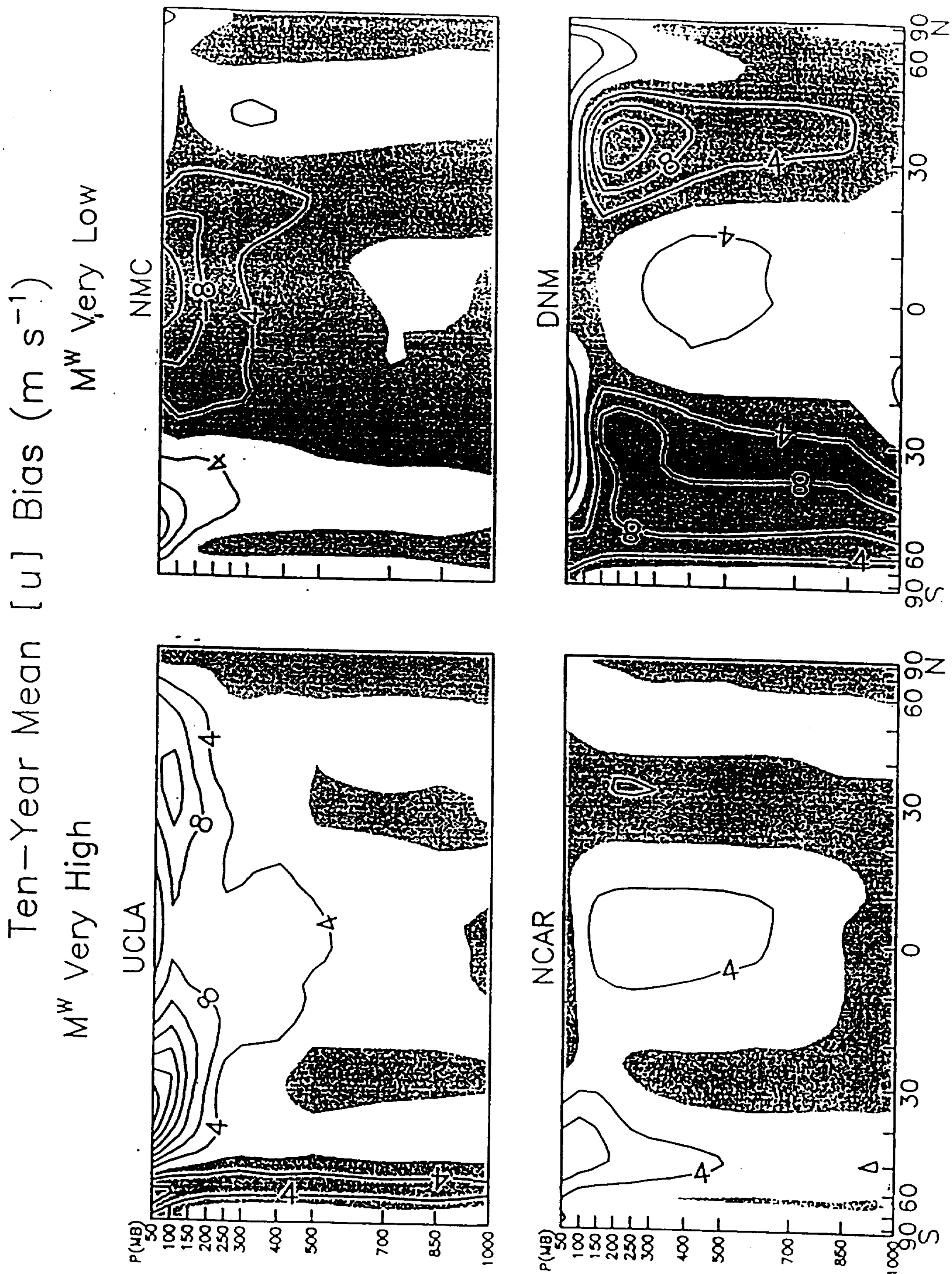

Ten-Year Mean [u] Bias (m s^{-1})
M^{W} Very High
M^{W} Very Low
UCLA
NMC
NCAR
DNM
P(MB)

Figure 5

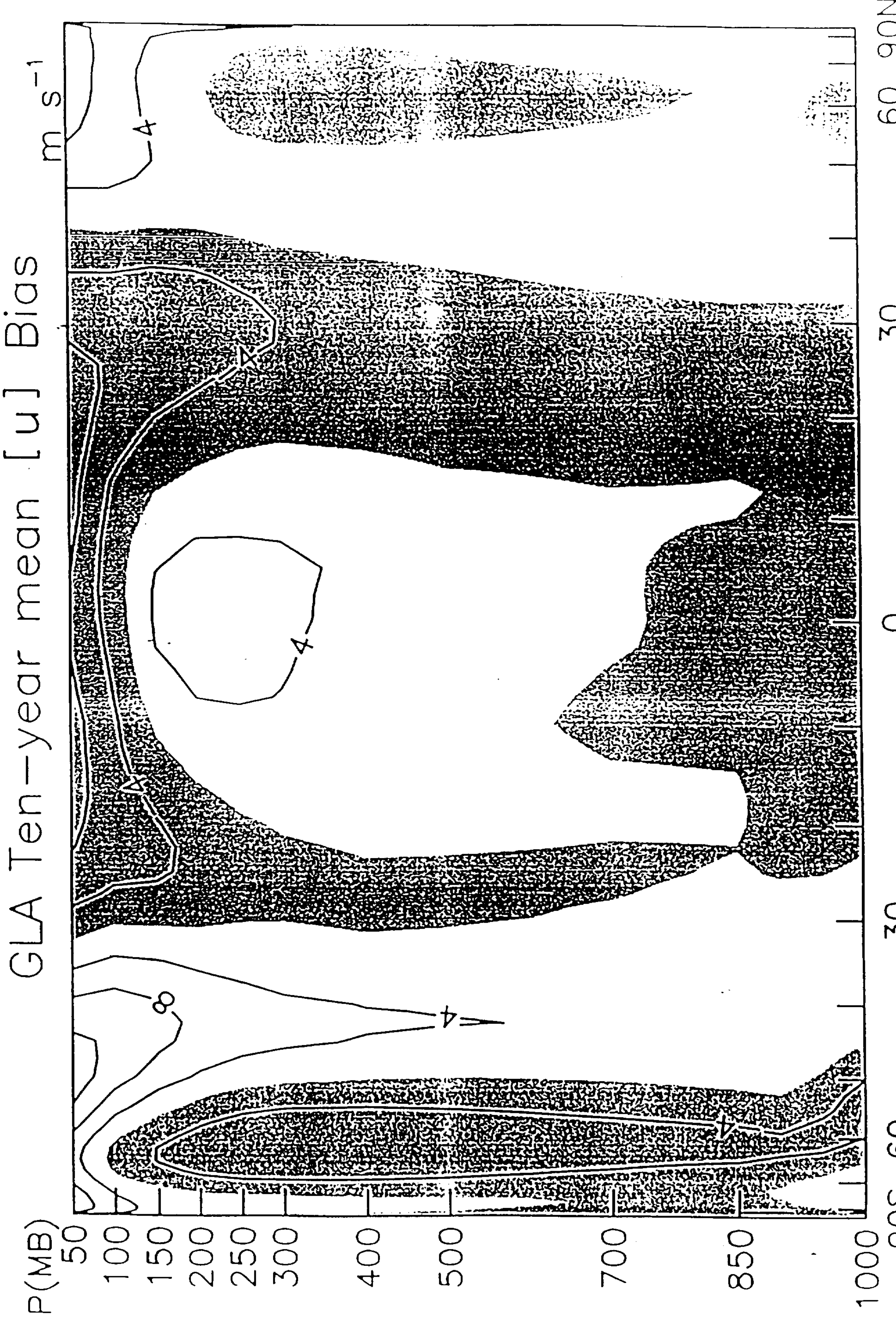
GLA Ten-year mean [u] Bias
m s-1
P(MB)
50
100
150
200
250
300
400
500
700
850
1000
90S
60
30
0
30
60
90N
4
-4
-8
-4
-4
4

Figure 6

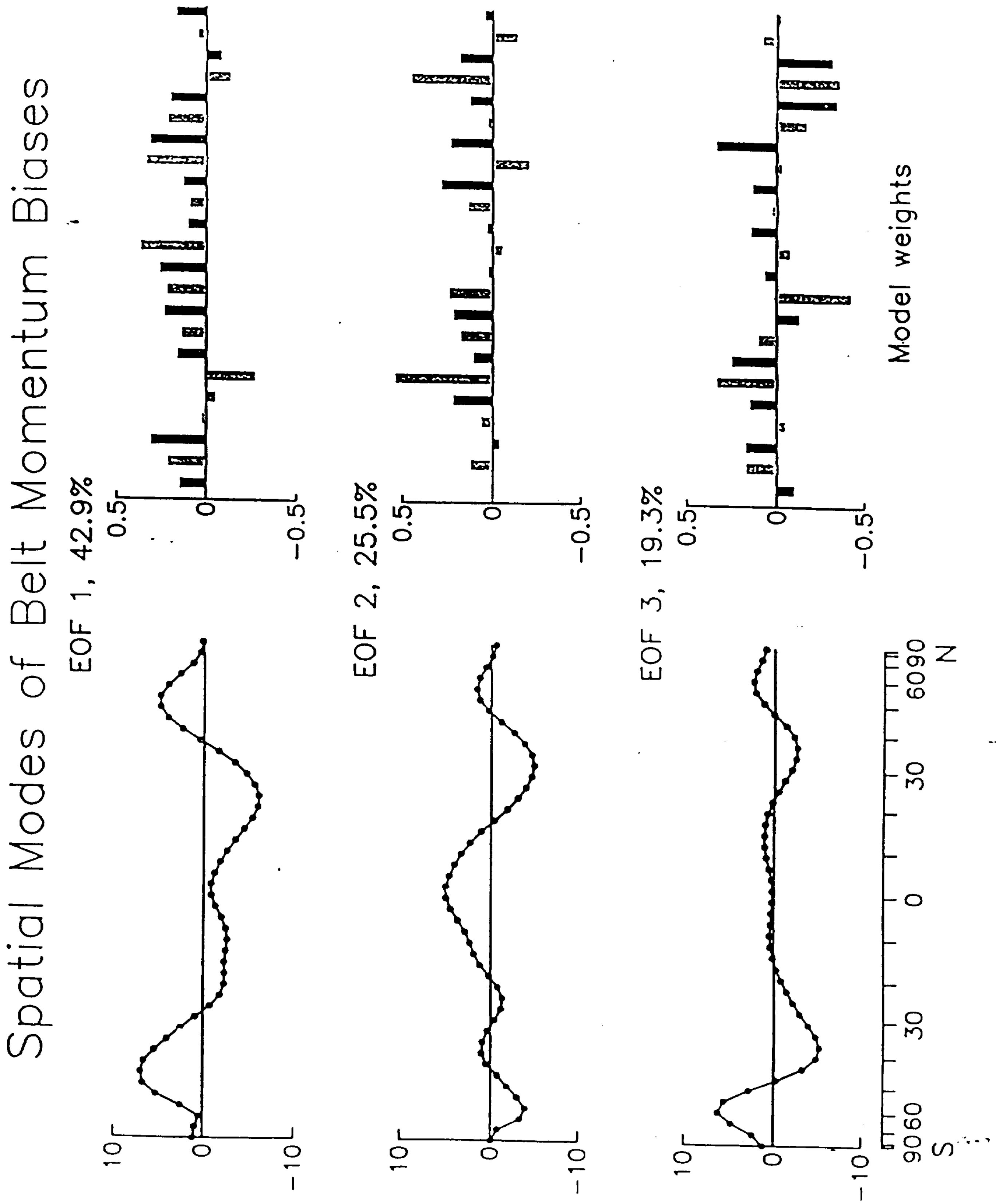

Spatial Modes of Belt Momentum Biases
EOF 1, 42.9%
EOF 2, 25.5%
EOF 3, 19.3%
10
0
−10
0.5
0
−0.5
90
60
30
0
30
60
90
S
N
Model weights

Figure 7

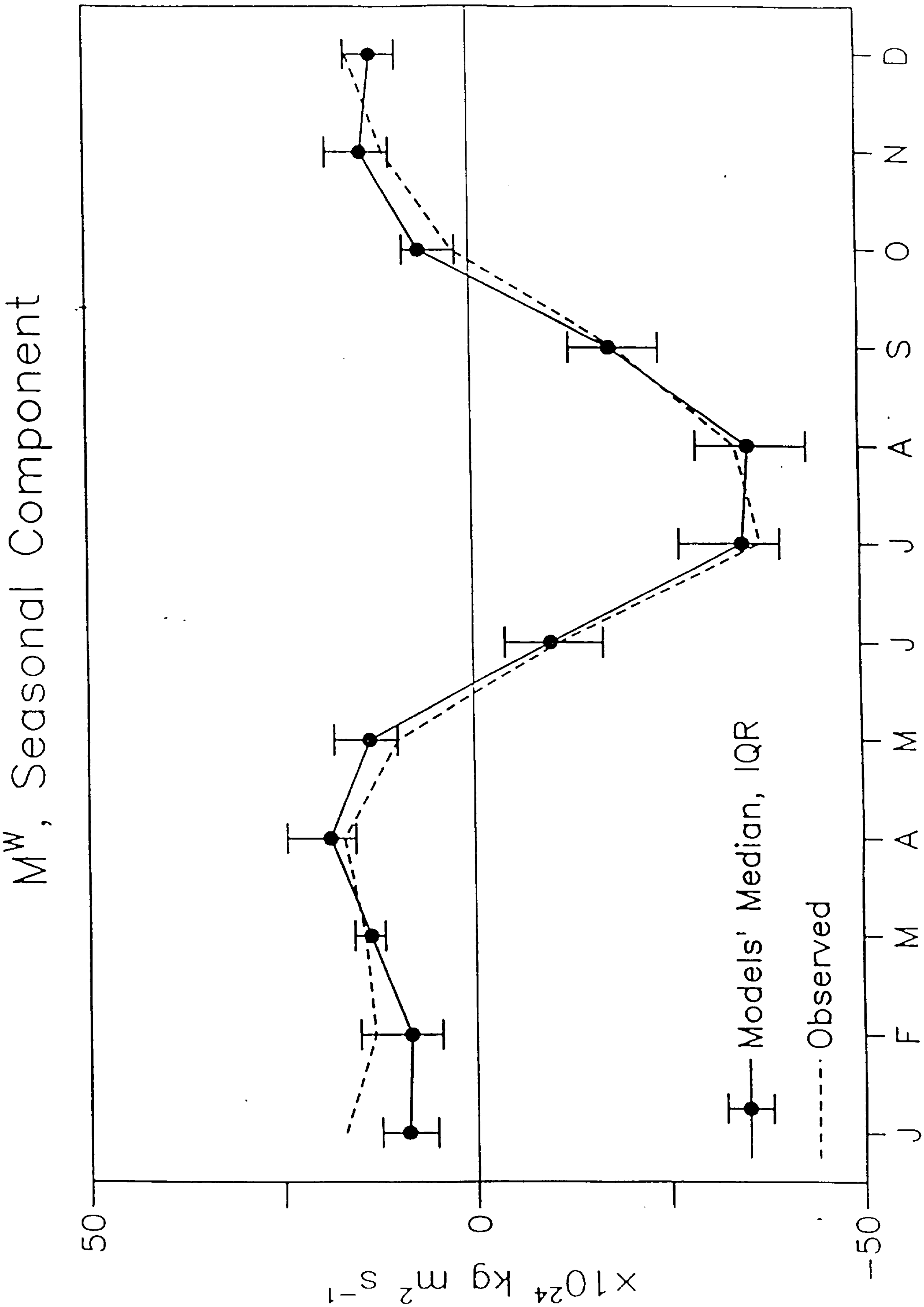

M^W, Seasonal Component
Models' Median, IQR
Observed
J F M A M J J A S O N D
50
0
−50
×10^24 kg m^2 s^-1

Figure 8

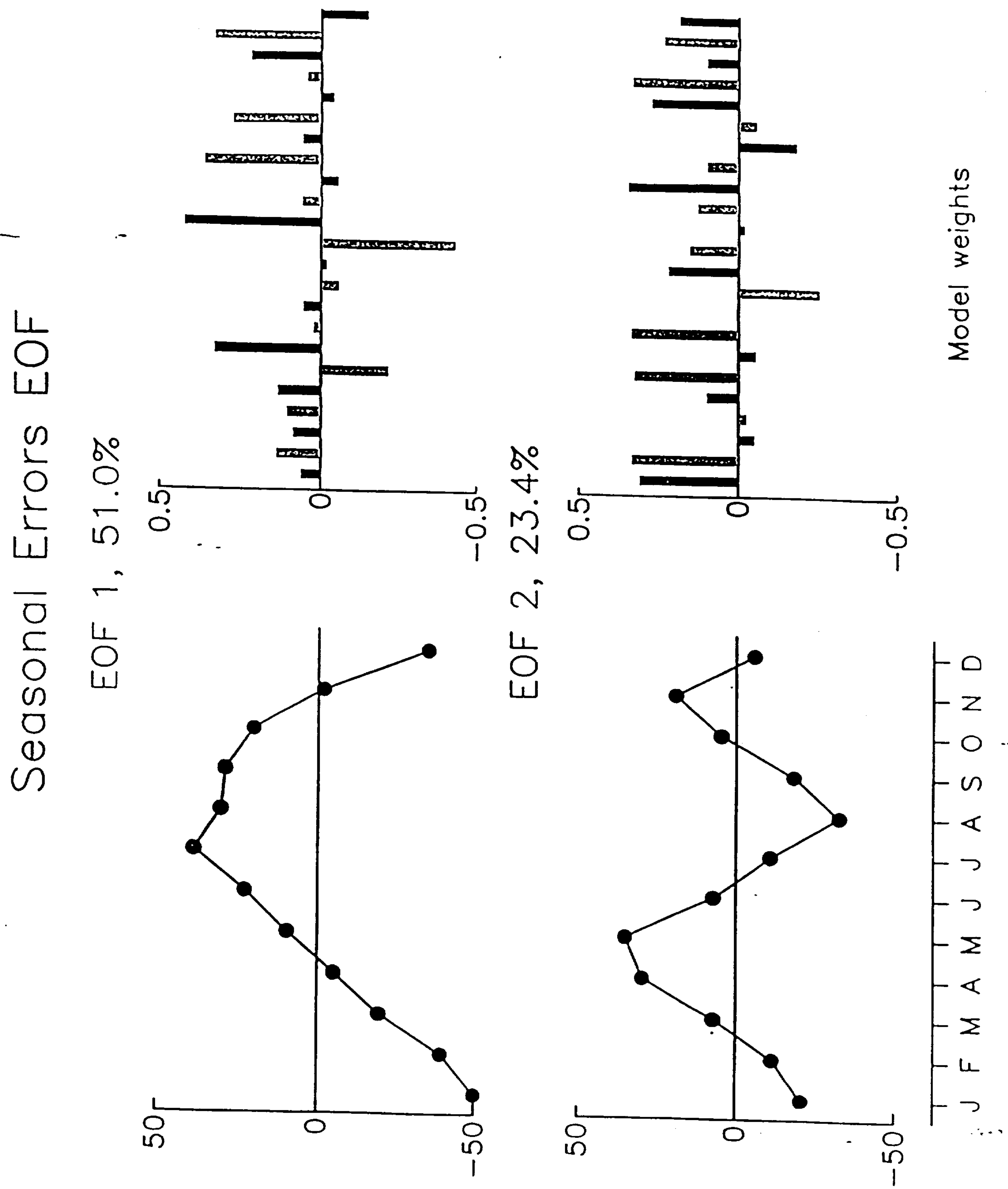

Seasonal Errors EOF
EOF 1, 51.0%
0.5
0
-0.5
50
0
-50
EOF 2, 23.4%
0.5
0
-0.5
50
0
-50
J F M A M J J A S O N D
Model weights

Figure 9

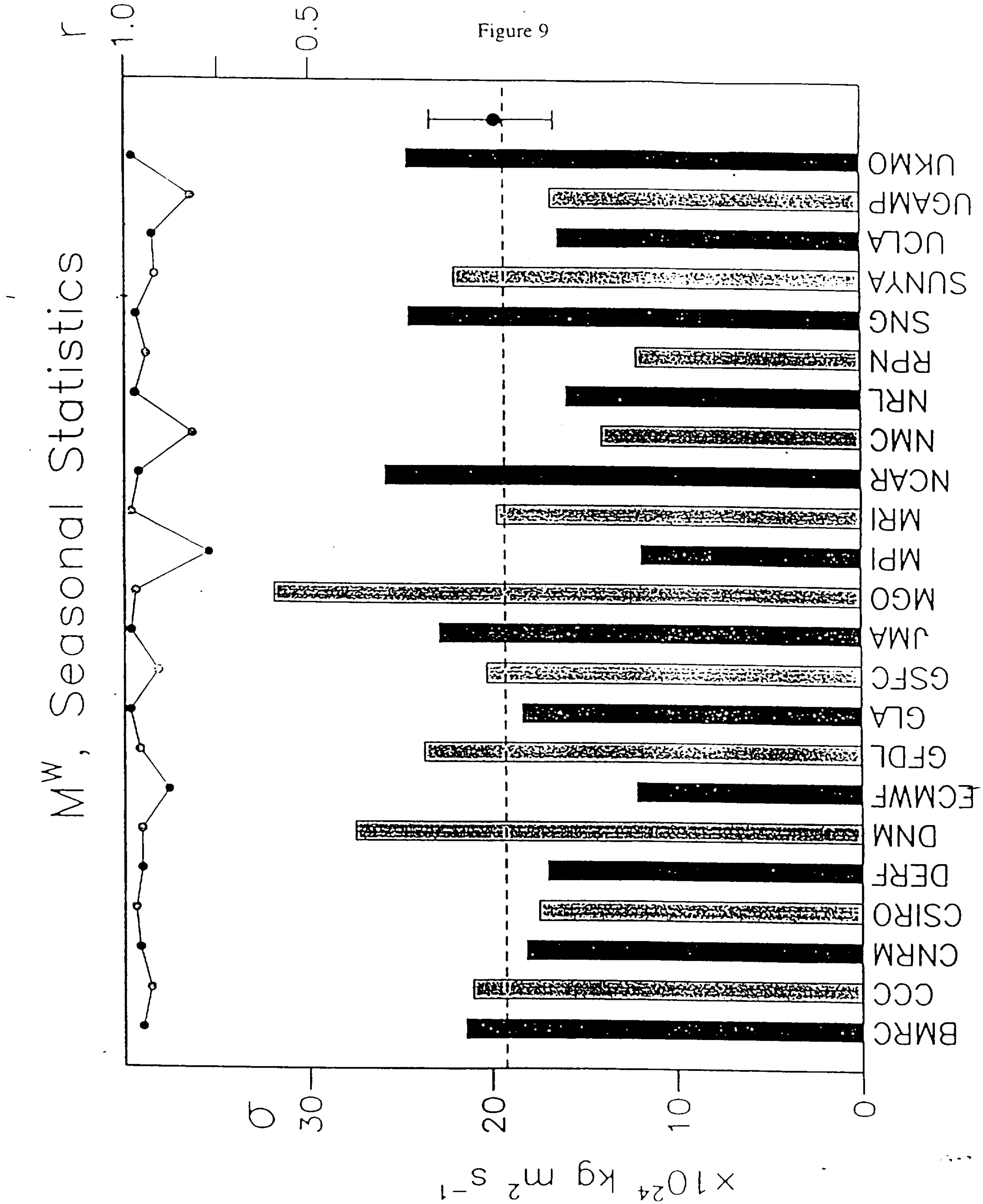

M^W, Seasonal Statistics
r
1.0
0.5
σ
30
20
10
0
×10^24 kg m^2 s^-1
BMRC
CCC
CNRM
CSIRO
DERF
DNM
ECMWF
GFDL
GLA
GSFC
JMA
MGO
MPI
MRI
NCAR
NMC
NRL
RPN
SNG
SUNYA
UCLA
UGAMP
UKMO

Figure 10a

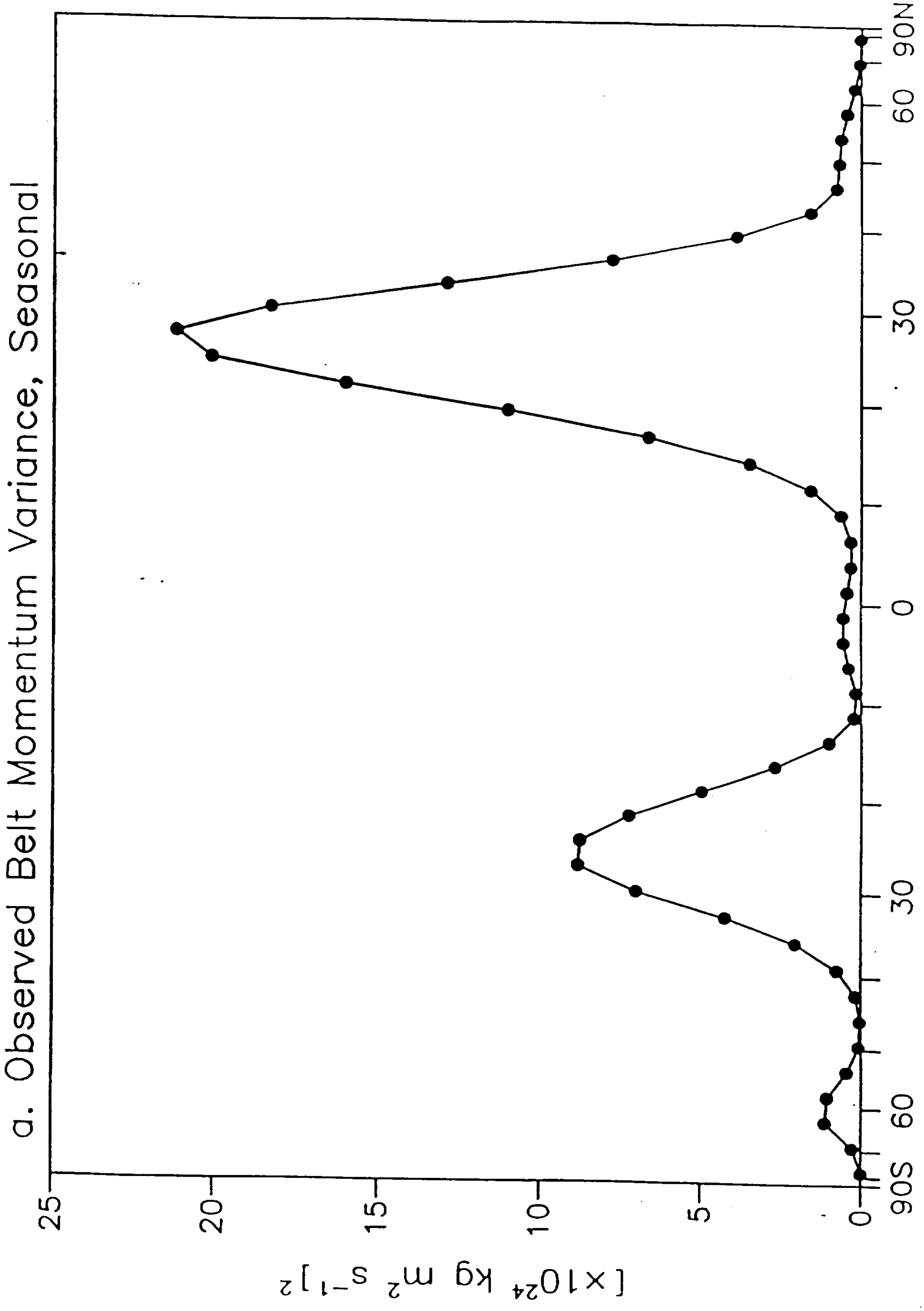
a. Observed Belt Momentum Variance, Seasonal
[×10^24 kg m^2 s^-1]^2
0
5
10
15
20
25
90S
60
30
0
30
60
90N

Figure 10b

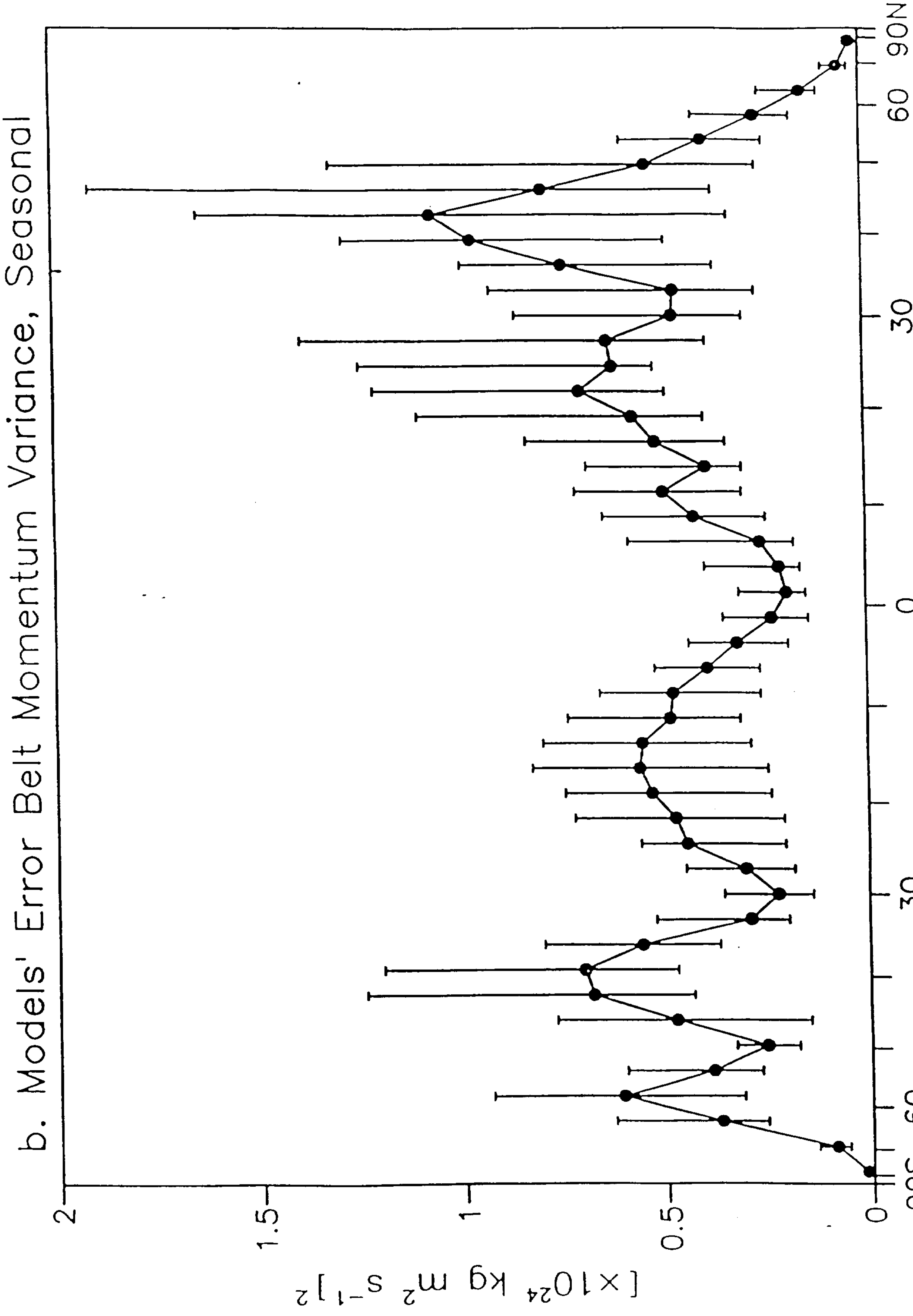

b. Models' Error Belt Momentum Variance, Seasonal
[×10²⁴ kg m² s⁻¹]²
2
1.5
1
0.5
0
90S
60
30
0
30
60
90N

Figure 10c

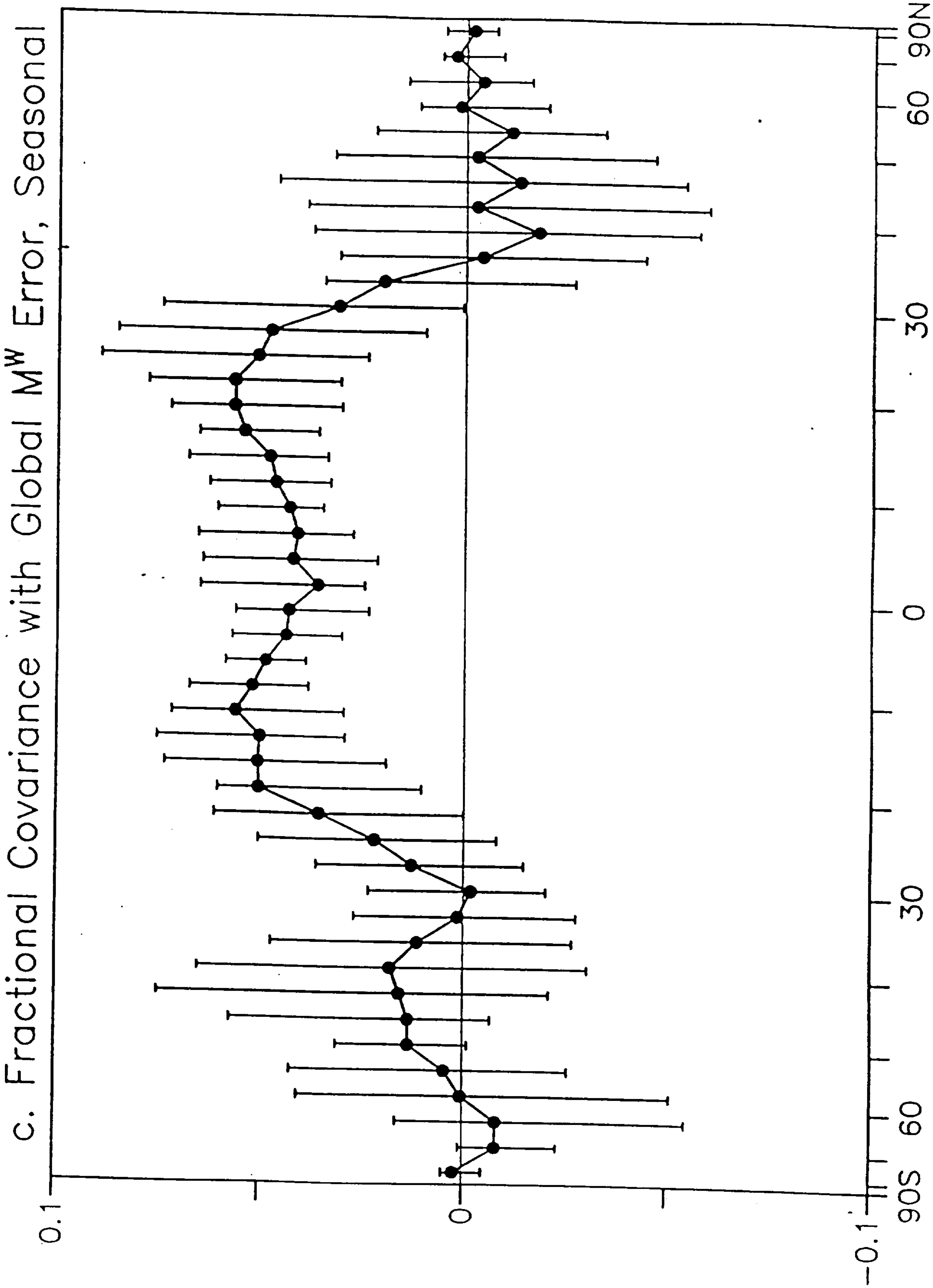
c. Fractional Covariance with Global M^W Error, Seasonal
0.1
0
-0.1
90S
60
30
0
30
60
90N

Figure 11

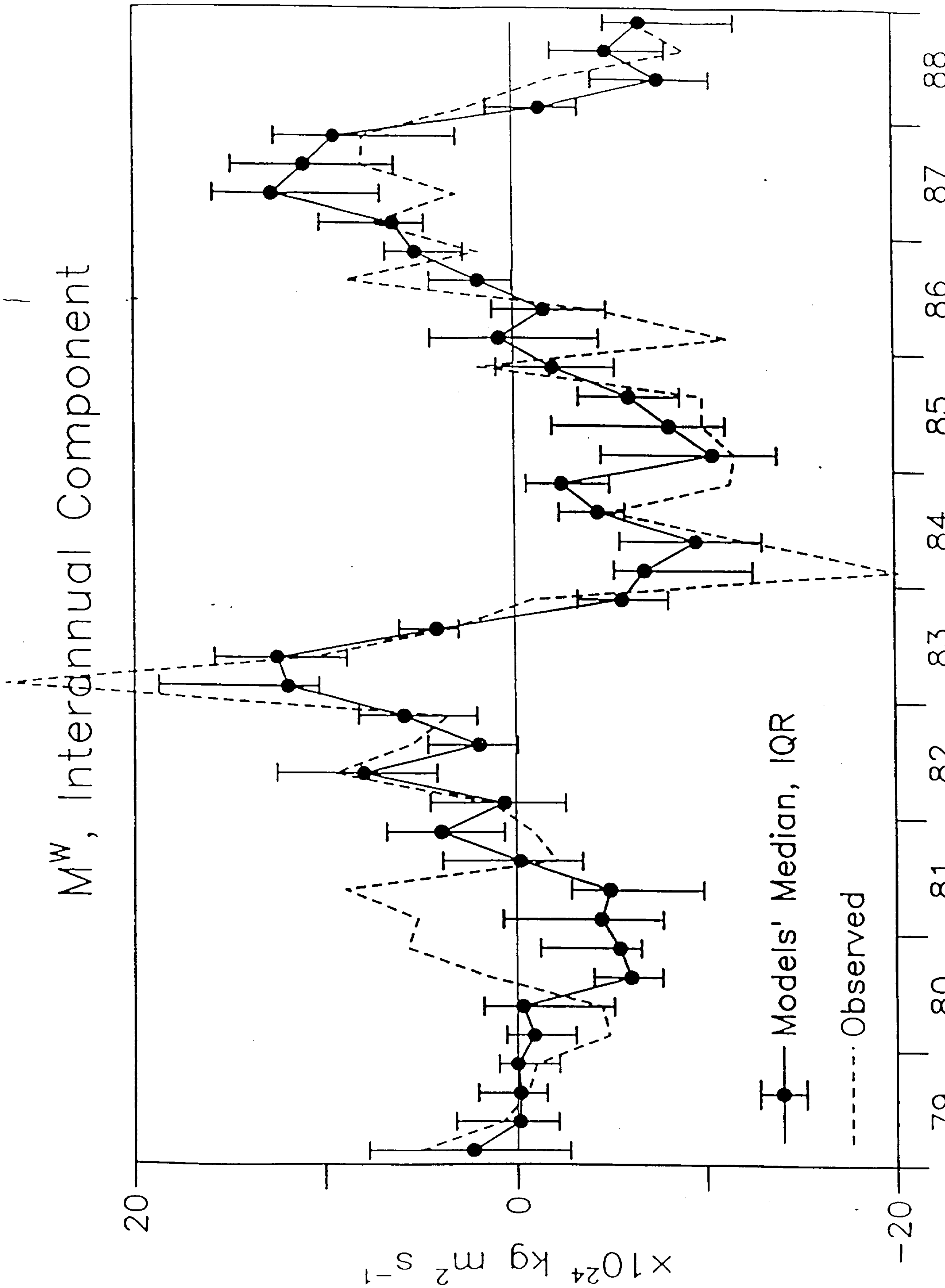

M^W, Interannual Component
Models' Median, IQR
Observed
$\times 10^{24}$ kg m^2 s^{-1}
20
0
−20
79
80
81
82
83
84
85
86
87
88

Figure 12

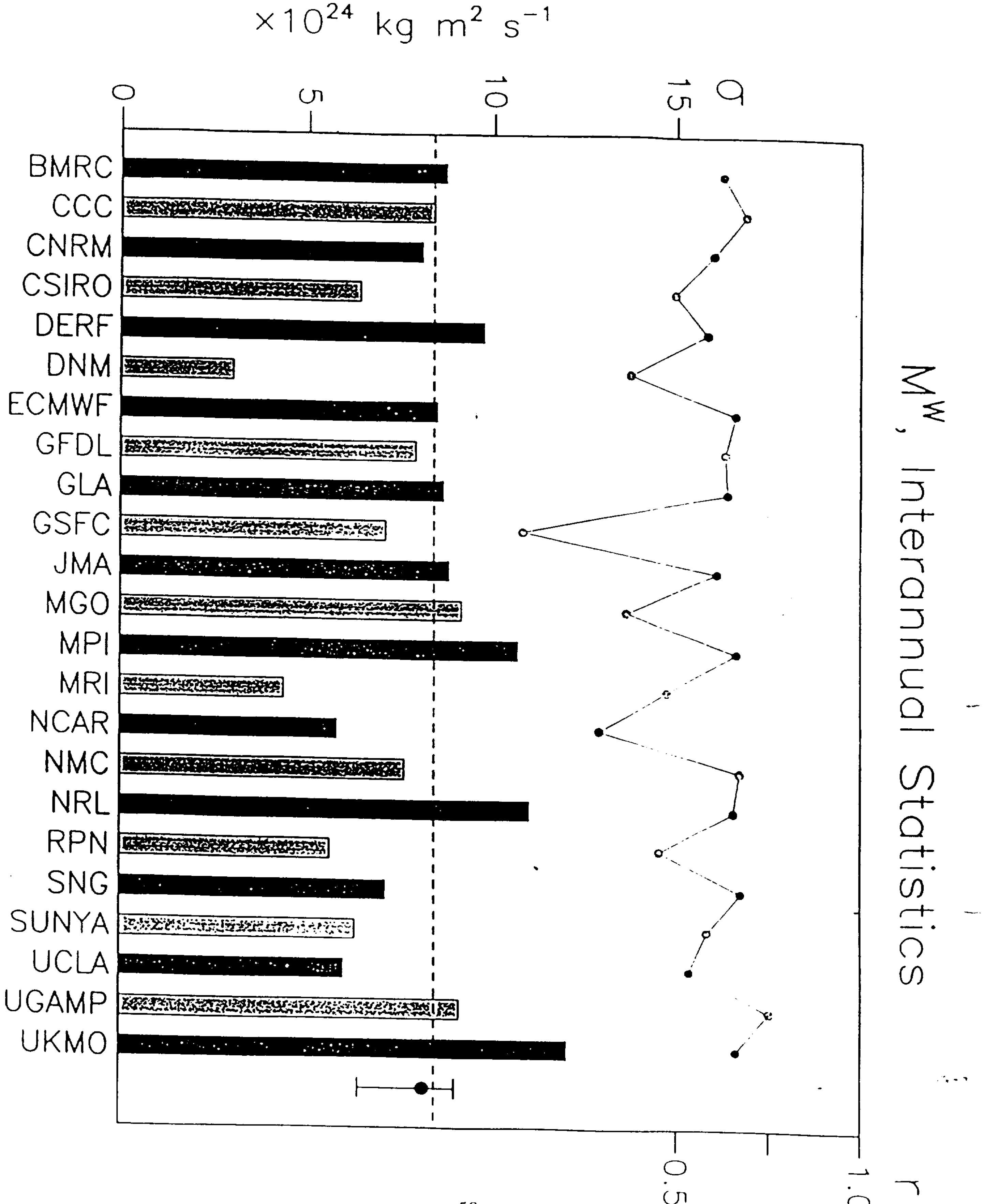

×10^24 kg m^2 s^-1
σ
0
5
10
15
BMRC
CCC
CNRM
CSIRO
DERF
DNM
ECMWF
GFDL
GLA
GSFC
JMA
MGO
MPI
MRI
NCAR
NMC
NRL
RPN
SNG
SUNYA
UCLA
UGAMP
UKMO
M^w, Interannual Statistics
r
0.5
1.0

Figure 13a

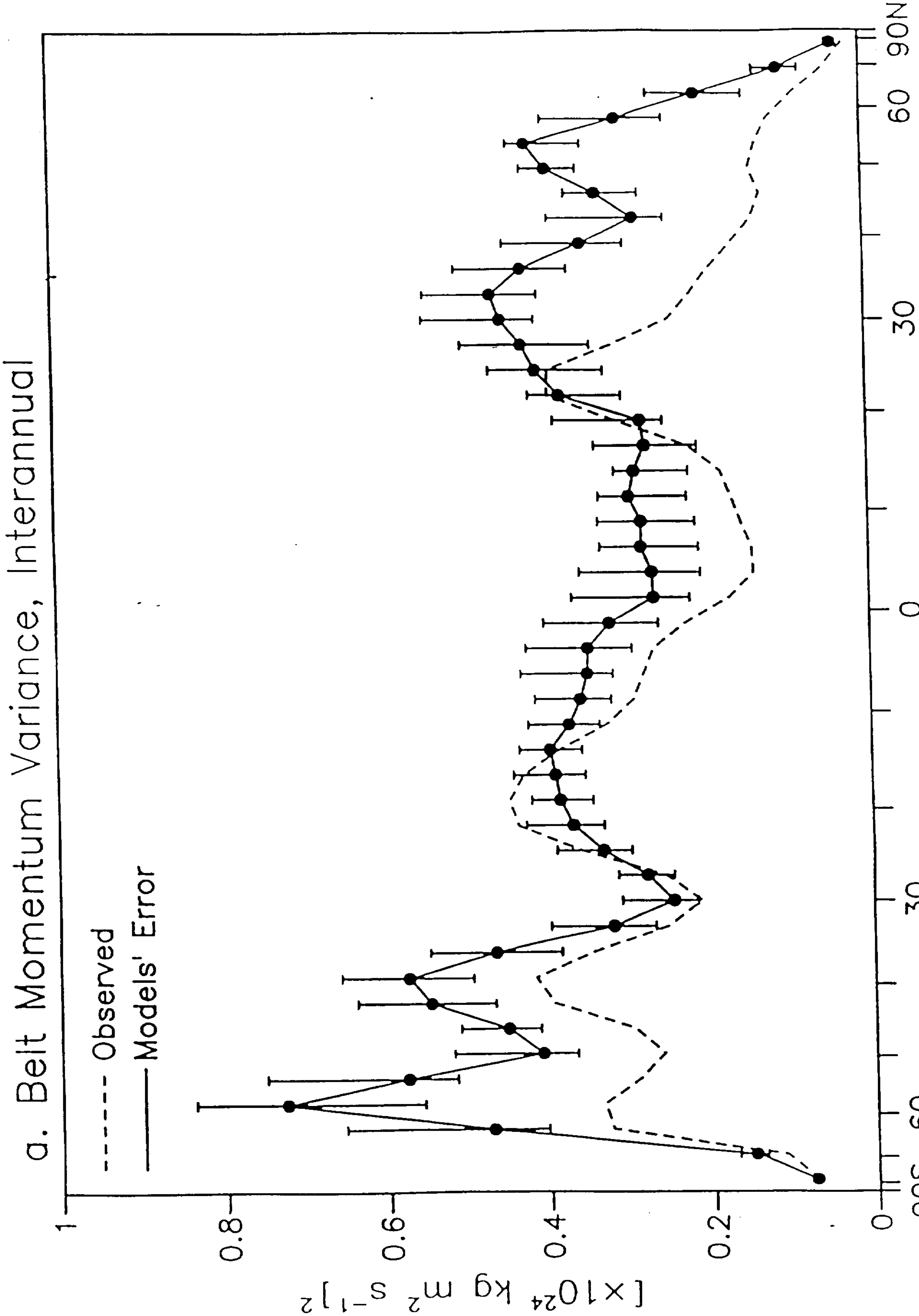

a. Belt Momentum Variance, Interannual
----- Observed
—— Models' Error
[×10²⁴ kg m² s⁻¹]²
0
0.2
0.4
0.6
0.8
1
90S
60
30
0
30
60
90N

Figure 13b

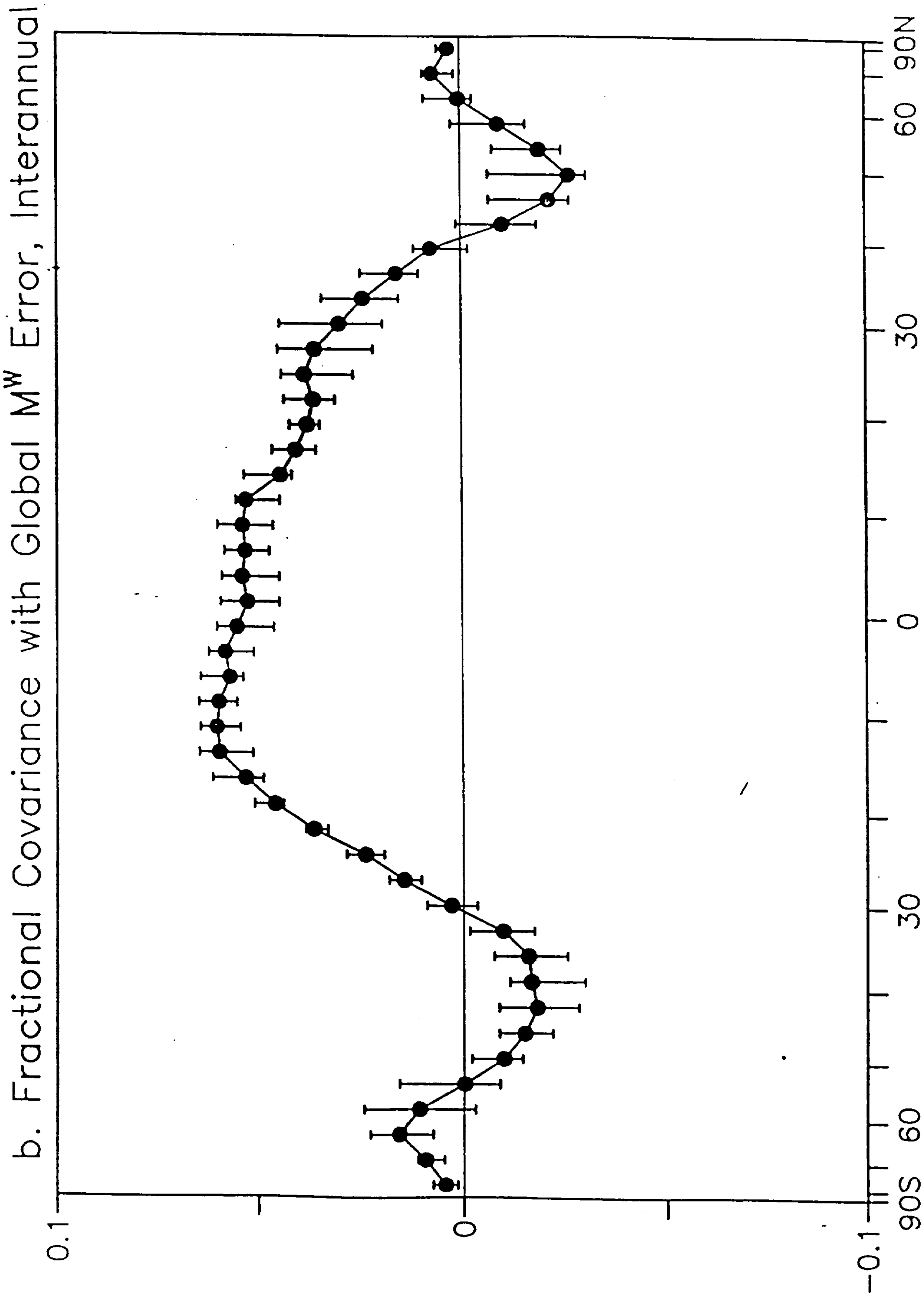

b. Fractional Covariance with Global M^W Error, Interannual
0.1
0
−0.1
90S
60
30
0
30
60
90N

Attachment 1

Relation between latent heating from the GEOS-1 Data Assimilation System and observed Outgoing Longwave Radiation

Haig Iskenderian and David Salstein
Atmospheric and Environmental Research, Inc., Cambridge, MA 02139

The zonally averaged latent heating anomalies for January 1987 and January 1989 from the GEOS-1 DAS system are shown in Fig. 1. There are notable differences between the two heating patterns. In January 1987 (Fig. 1a), there is anomalous heating centered about the equator. This area of greater than normal heating is flanked by negative heating anomalies in both the Northern and Southern Hemispheres, centered on about 15°N and 15°S respectively. Anomalously high latent heating exists in the midlatitudes near 40°N and 50°S. The latent heating profile in January 1989 (Fig. 1b) is essentially a mirror image of the profile in January 1987. Anomalously low values of latent heating are centered near the equator, while anomalously high latent heating is positioned in the subtropics of both Hemispheres near 20°N and 20°S. Negative heating anomalies prevail in the midlatitudes of both Hemispheres.

In order to better determine which portions of the globe contribute to this observed difference in zonally averaged latent heating in the Tropics and subtropics, Fig. 2 displays the difference of the vertically averaged GEOS-1 DAS latent heating between the two Januarys. The trapezoidal rule was used to perform the vertical average which extends from the surface to 20 hPa. It is readily seen that the largest difference between the two Januarys is over the low latitudes of the central and western Pacific. Along the equator, there is less heating indicated in the central and western Pacific in 1989 relative to 1987. This area of reduced heating is flanked to the north and south by regions of greater heating in 1989 relative to 1987 over the subtropics of the central and western Pacific along about 20°N and 20°S. Hence it appears that the region of the tropical and subtropical central and western Pacific contributes most to the zonally averaged anomalies in Fig. 1.

This difference of latent heating between the two Januarys is possibly related to a shift of convective activity in the tropical Pacific connected with the El Niño/Southern Oscillation (ENSO) phenomenon. During January 1987 there was a warm ENSO event

(Kousky 1987), and January 1989 was associated with a cool phase of ENSO (Arkin 1989). The shift of convective activity is shown by comparing the Outgoing Longwave Radiation (OLR) anomaly fields between January 1987 and January 1989 (Fig. 3). OLR has been shown to be an effective proxy for convective activity in the Tropics and subtropics. The anomalies are computed from an 8 yr. (1986-1993) reference period. The OLR data is from National Oceanic and Atmospheric Administration (NOAA) polar orbiting satellites (Gruber and Krueger 1984), and is provided by the National Center for Atmospheric Research (NCAR). Fig. 3a shows that during January 1987, above normal convective activity (negative OLR anomalies) is observed in the central Pacific near 160°W along the equator, while below normal convection (positive OLR anomalies) exists in the western Pacific near 150°E. This is in contrast to January 1989 (Fig. 3b), when above normal convective activity is observed in the western Pacific, and below normal convective activity is observed over the central Pacific.

Since convection is directly associated with diabatic heating in the atmosphere, we expect that areas of anomalous convection correspond to areas of anomalously high latent heating. Fig. 4 shows the vertically averaged GEOS-1 DAS latent heating anomalies for January 1987 and January 1989. The anomalies are computed from the same 1986-1993 base period as the OLR anomalies in Fig. 3. In January 1987, anomalously high latent heating is indicated in the central Pacific near 160°W, associated with the anomalous convection there. Negative anomalies are observed over the western Pacific near 150°E, consistent with reduced convection in this region. In January 1989, negative heating anomalies are observed over the central Pacific, consistent with the anomalously high values of OLR over the region, which is indicative of less than normal convective activity. The positive latent heating anomalies are confined to the subtropics.

The spatial correlation between OLR anomalies and vertically averaged heating anomalies is computed in order to further establish the relationship between convection and the GEOS-1 based latent heating in the tropical Pacific region. The region is defined as bounded by 30°S and 30°N latitude, and 100°E and 120°W longitude. The scatter diagrams (not shown) indicate a negative correlation in the tropical Pacific for all years, with a stronger negative correlation (-0.63) for 1989 relative to 1987 (-0.42). Temporal correlation is then computed globally for all eight Januarys, Aprils, Julys, and Octobers to investigate whether this negative correlation between OLR and latent heating holds for the entire sample. The results are shown in Fig. 5. Overall, there is a tendency for a negative correlation between latent heating and OLR globally. In January (Fig. 5a), the highest negative correlation and largest spatial extent of high negative correlation in the tropical belt is found in the central Pacific, and over northern Australia. This region shows a statistical significance of 95% which is indicated by the shading in Fig. 5. In April (Fig. 5b), the area of high negative correlation in the tropical belt extends farther eastward to the west coast of South America. The area remains in the central Pacific in July (Fig. 5c), and is practically non-existent in October (Fig. 5d).

In summary, these results show that there is a considerable negative correlation between anomalous convection as indicated by the NOAA OLR fields and latent heating from the GEOS-1 DAS assimilation. The negative correlation between the two independent datasets indicates that the GEOS-1 DAS assimilation is accurately capturing the gross features of the latent heating associated with Tropical convection. This correlation is robust throughout a large portion of the year, particularly in the cool months of the Northern Hemisphere. Furthermore, the GEOS-1 DAS assimilation apparently captures some of the interannual variability of convective activity (and latent heating) due to the ENSO cycle of 1987-1989.

References:

Arkin, P.A., 1989: The global climate for December 1988-February 1989: Cold episode in the tropical Pacific continues. *J. Climate*, **2**, 737-757.

Gruber, A. and A.F. Krueger, 1984: The status of the NOAA outgoing longwave radiation data set. *Bull. Amer. Meteor. Soc.*, **65**, 958-962.

Kousky, V.E., 1987: The global climate for December 1986-February 1987: El Niño returns to the tropical Pacific. *Mon. Wea. Rev.*, **115**, 2822-2838.

Figures:

Fig. 1. Zonally averaged latent heating anomaly (deg day^{-1}) for (a) January 1987 and (b) January 1989. Contour interval is 0.1, and negative values are shaded.

Fig. 2. Difference of vertically averaged latent heating (deg day^{-1}) between January 1989 and January 1987. Contour interval is 1, negative (positive) values are dashed (solid). The zero line has been omitted.

Fig. 3. NOAA OLR anomalies (W m^{-2}) for (a) January 1987 and (b) January 1989. Contour interval is 10 and negative (positive) values are dashed (solid). The zero line has been omitted.

Fig. 4. GEOS-1 DAS vertically averaged latent heating anomalies (deg day^{-1}) for (a) January 1987 and (b) January 1989. Contour interval is 0.5 and negative (positive) values are dashed (solid). The zero line has been omitted.

Fig. 5. Composite correlation coefficient between OLR anomalies and vertically averaged latent heating anomalies for (a) January, (b) April, (c) July, and (d) October 1986 to 1993. Contours are drawn for values of 0.8, 0.6, -0.6, and -0.8, with negative (positive) values dashed (solid). Values less than -0.7 (95% significance level) are shaded.

deg/day

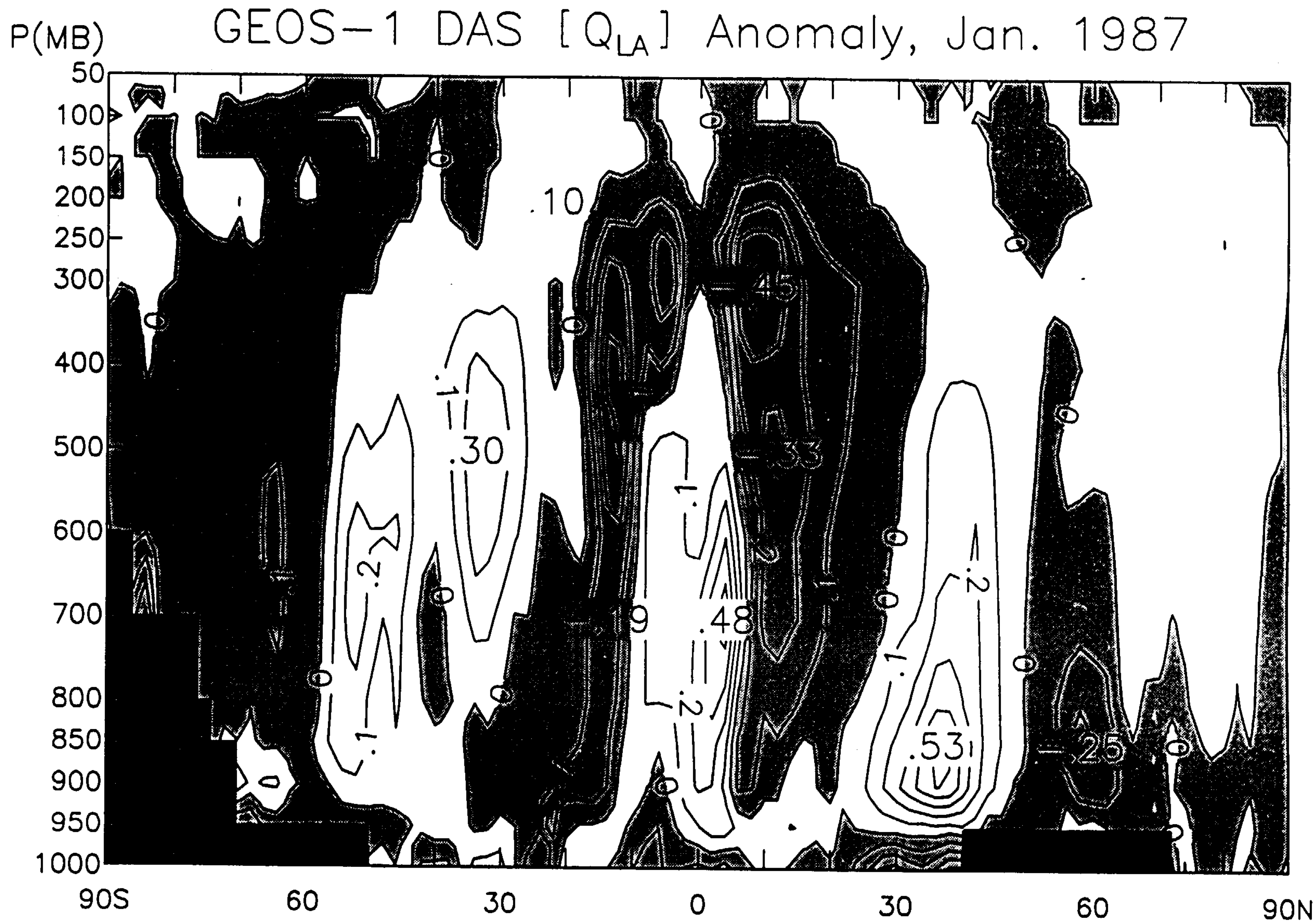

Fig. 1a

deg/day

GEOS-1 DAS [Q_{LA}] Anomaly, Jan. 1989

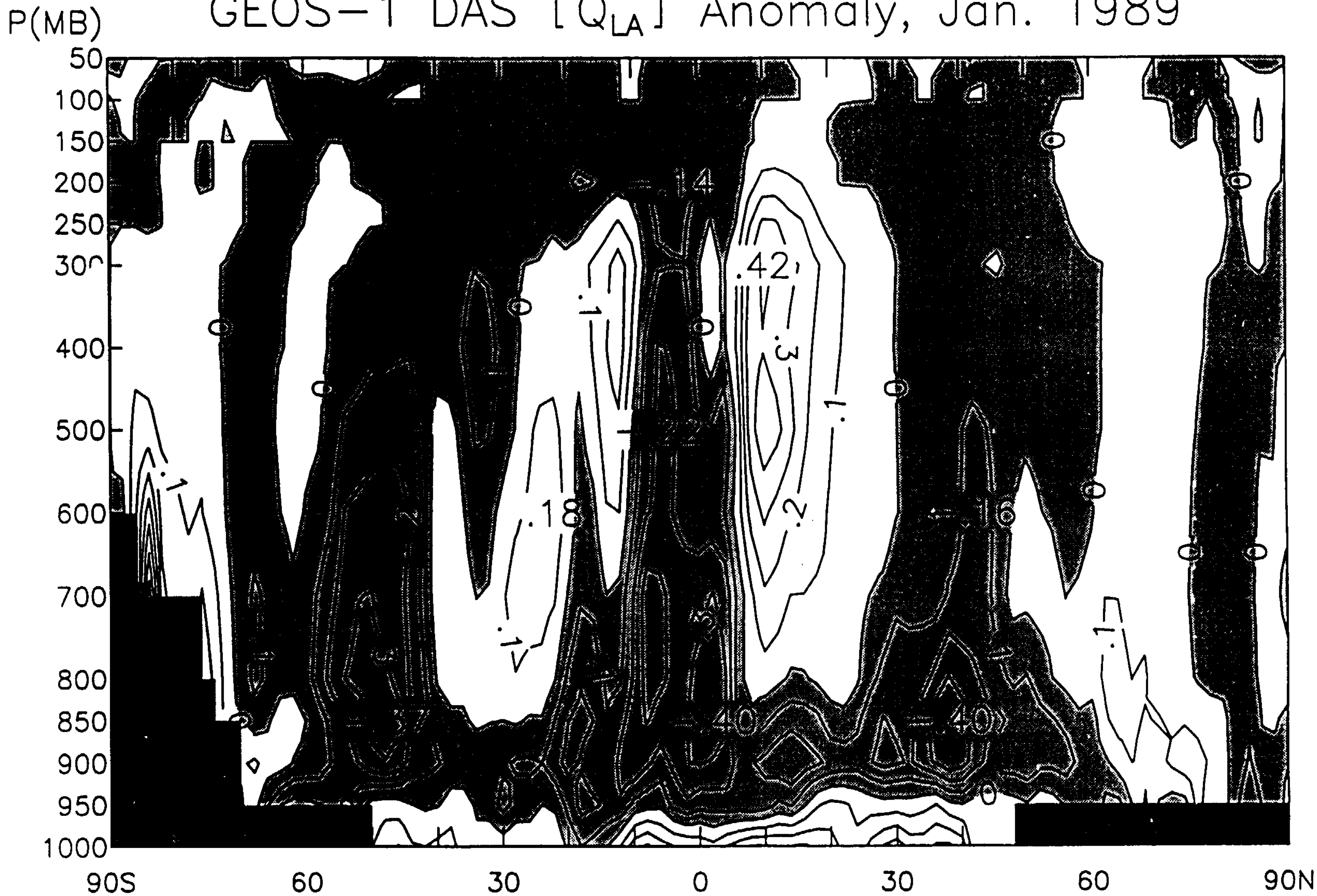

Fig. 6

Jan 1989 minus Jan 1987
GEOS-1 DAS VAVGQLA (Deg/day)

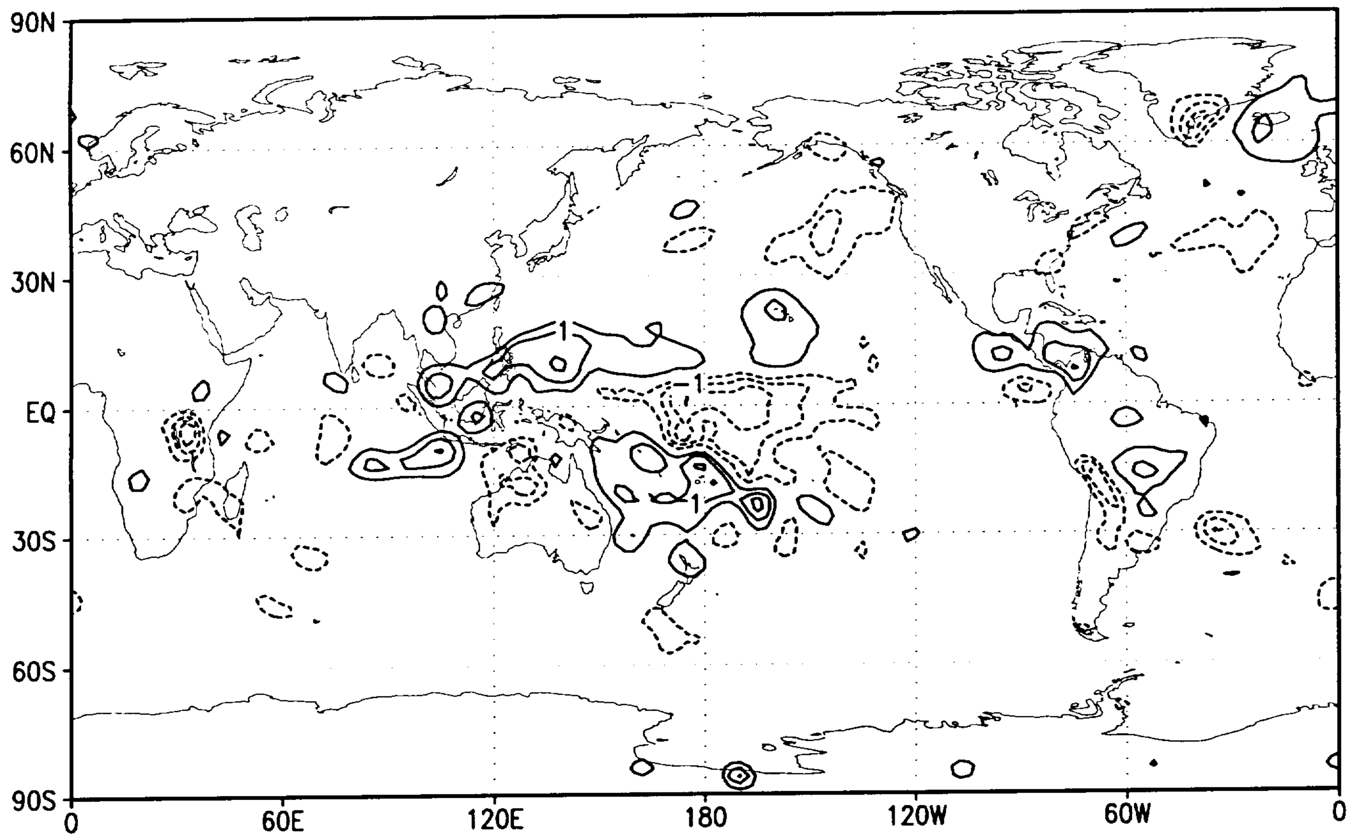

Jan 1987 NOAA OLR minus
8yr climatology (W/m**2)

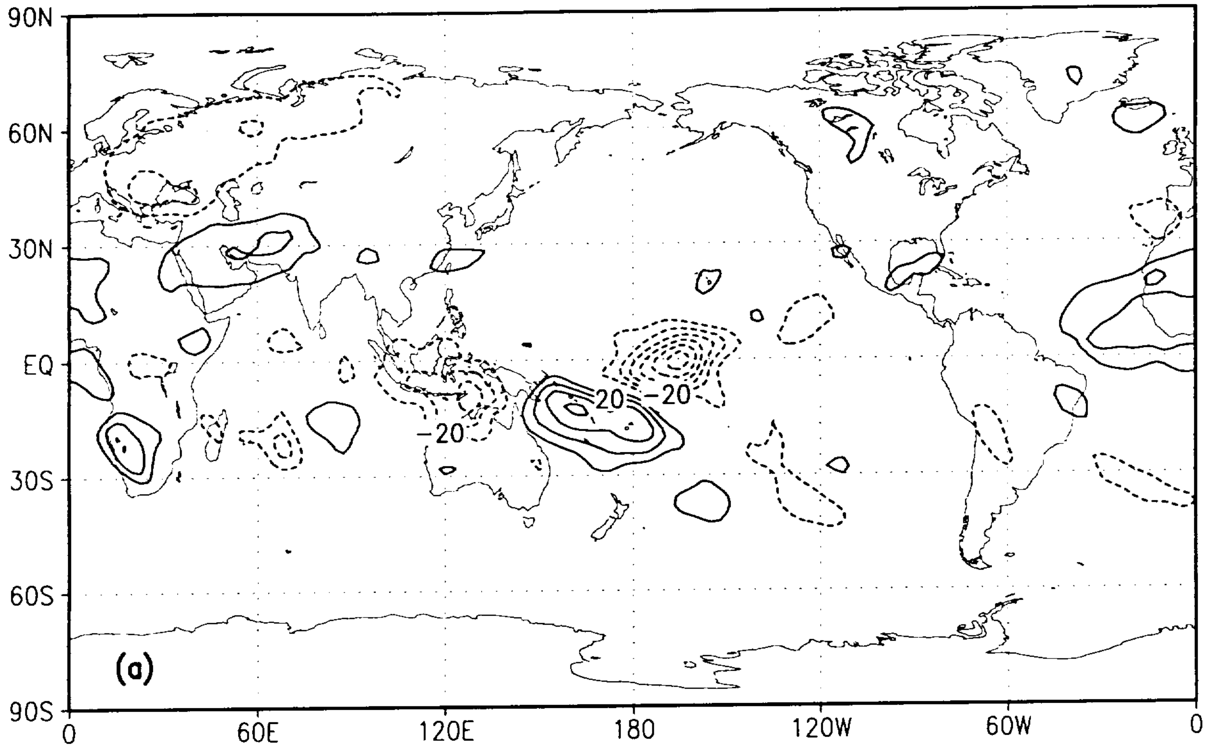

Jan 1989 NOAA OLR minus
8yr climatology (W/m**2)

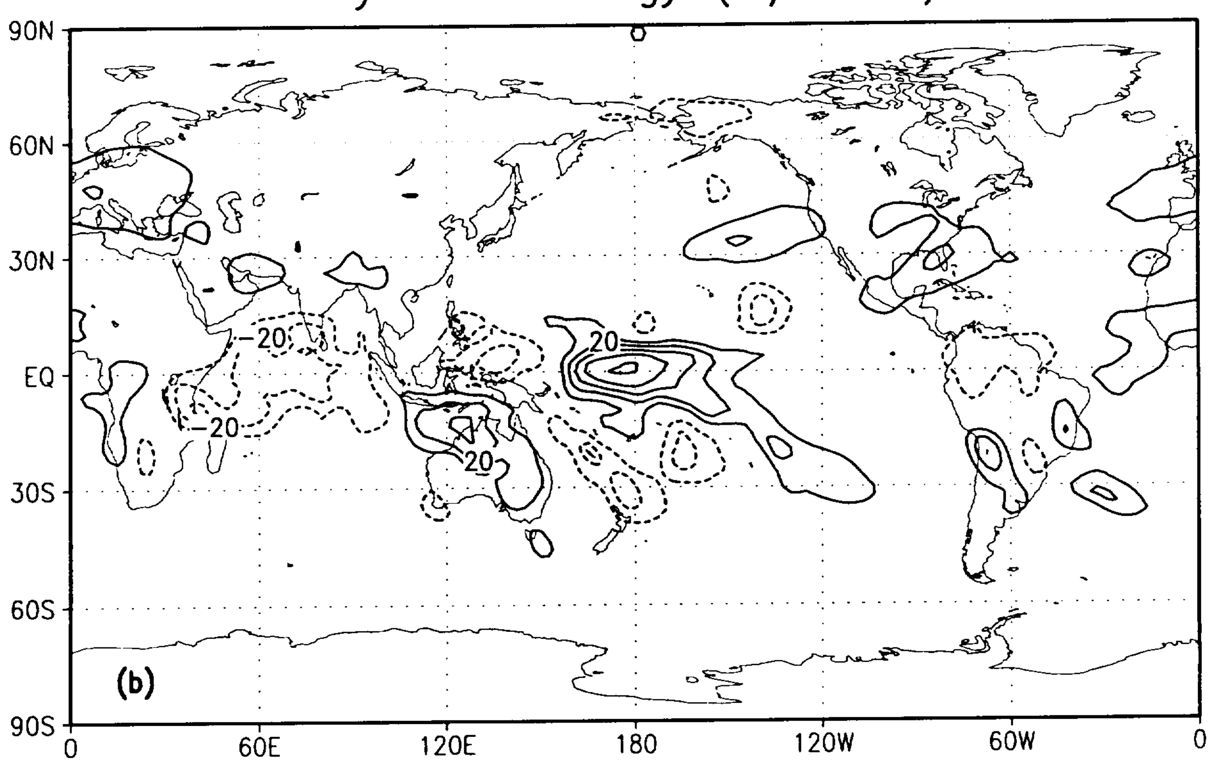

Fig. 3

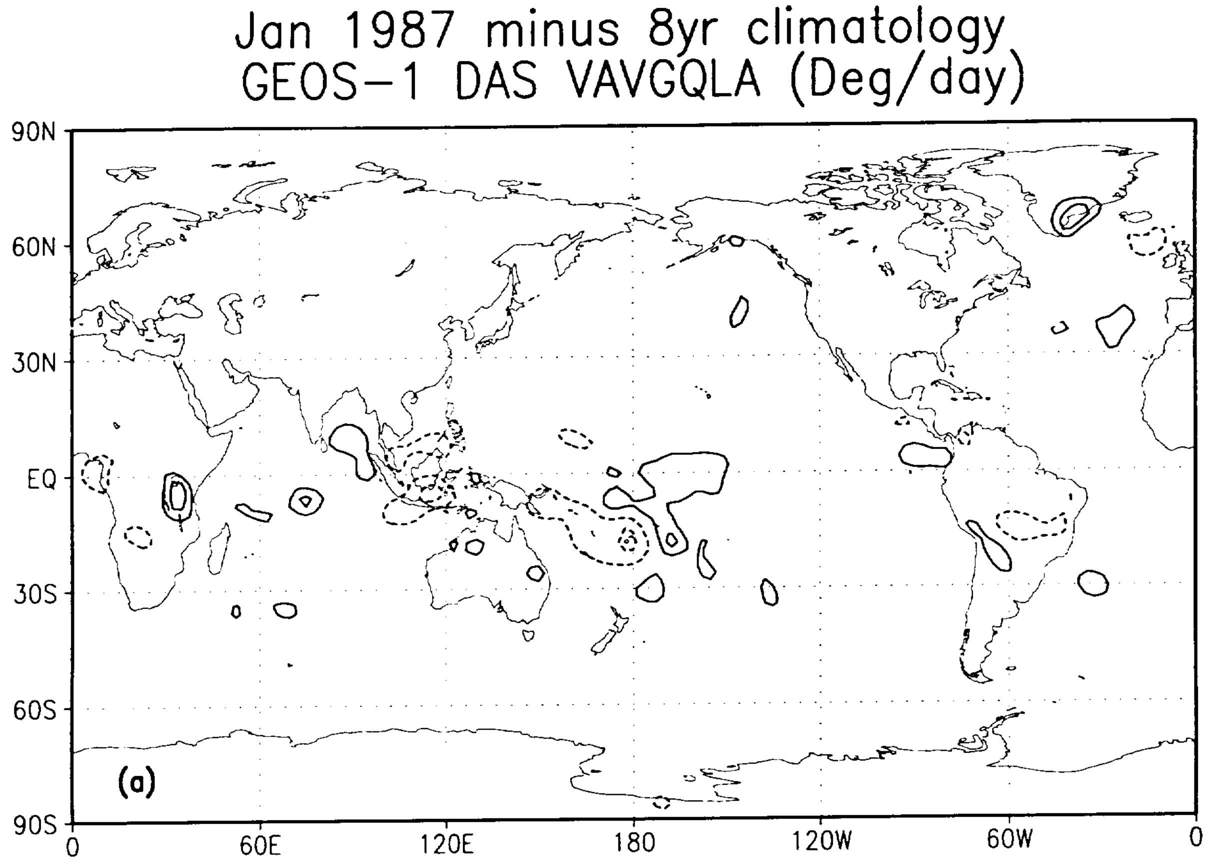
Jan 1987 minus 8yr climatology
GEOS-1 DAS VAVGQLA (Deg/day)
90N
60N
30N
EQ
30S
60S
90S
0
60E
120E
180
120W
60W
0
(a)

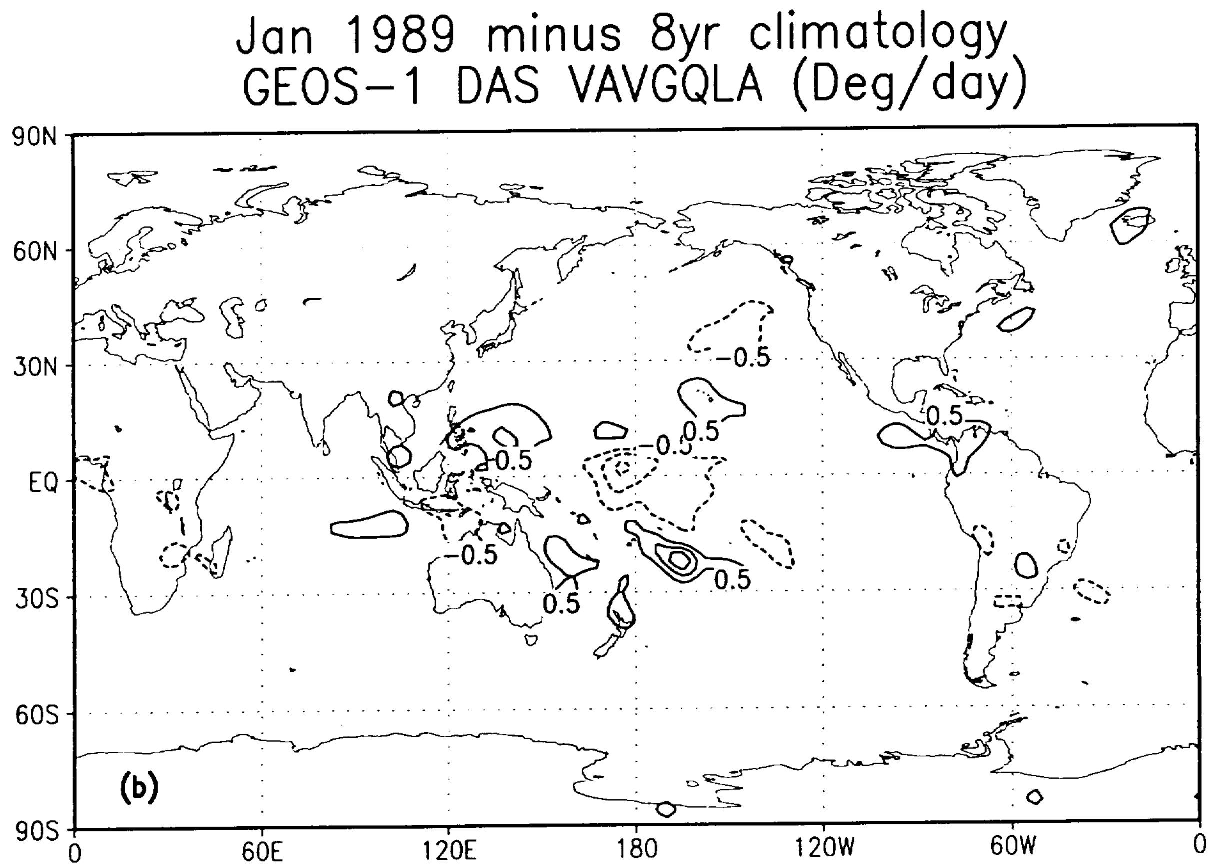
Jan 1989 minus 8yr climatology
GEOS-1 DAS VAVGQLA (Deg/day)
90N
60N
30N
EQ
30S
60S
90S
0
60E
120E
180
120W
60W
0
-0.5
0.5
(b)

January 1986–93 corr. VAVGQLA' and OLR'

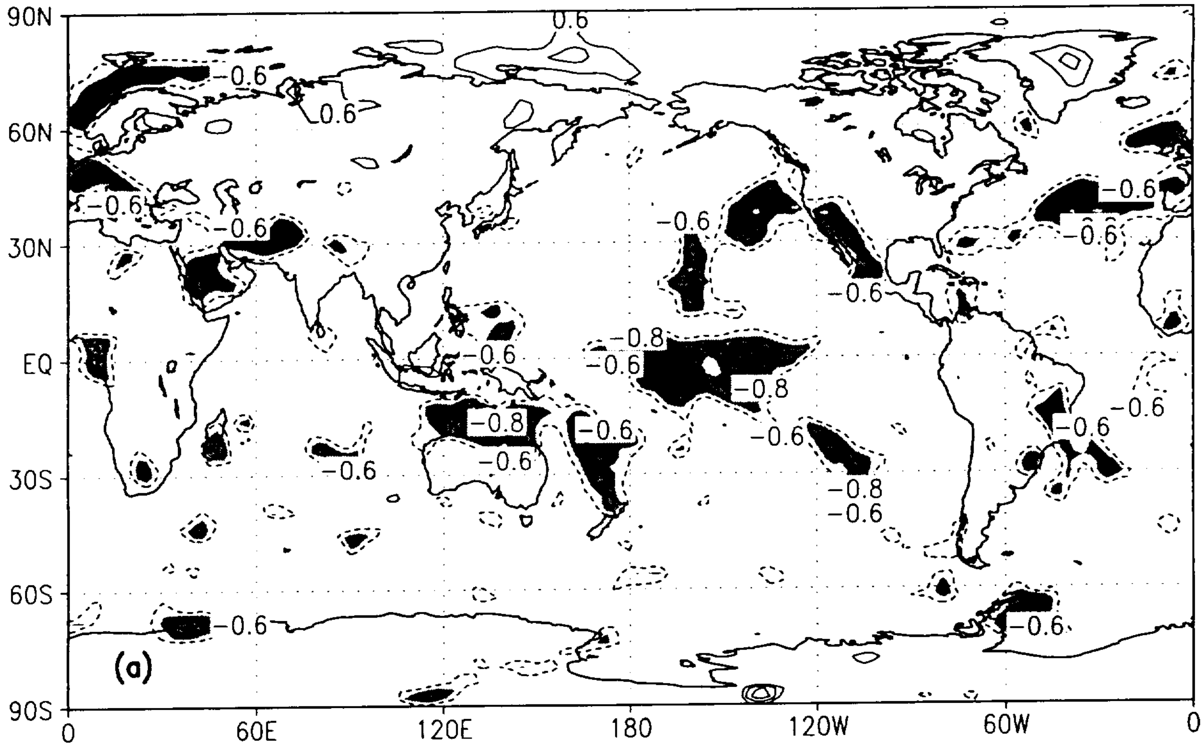

April 1986–93 corr. VAVGQLA' and OLR'

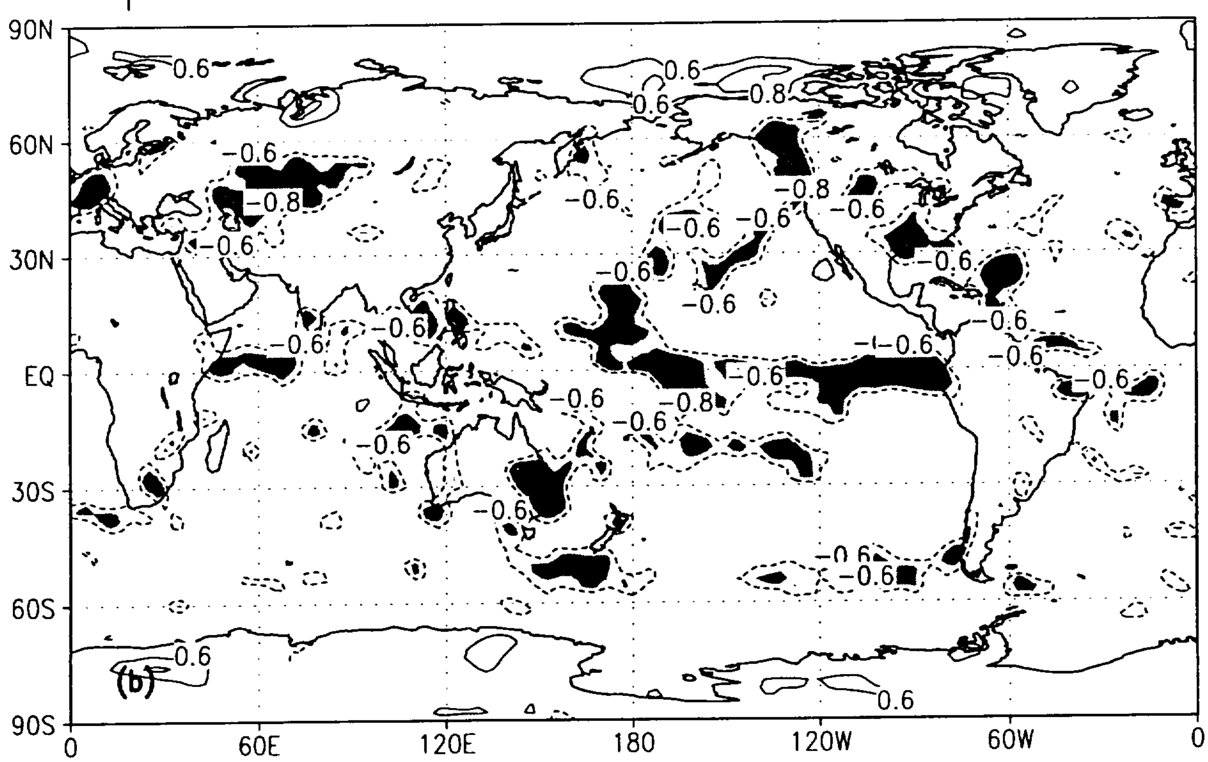

July 1986–93 corr. VAVGQLA' and OLR'

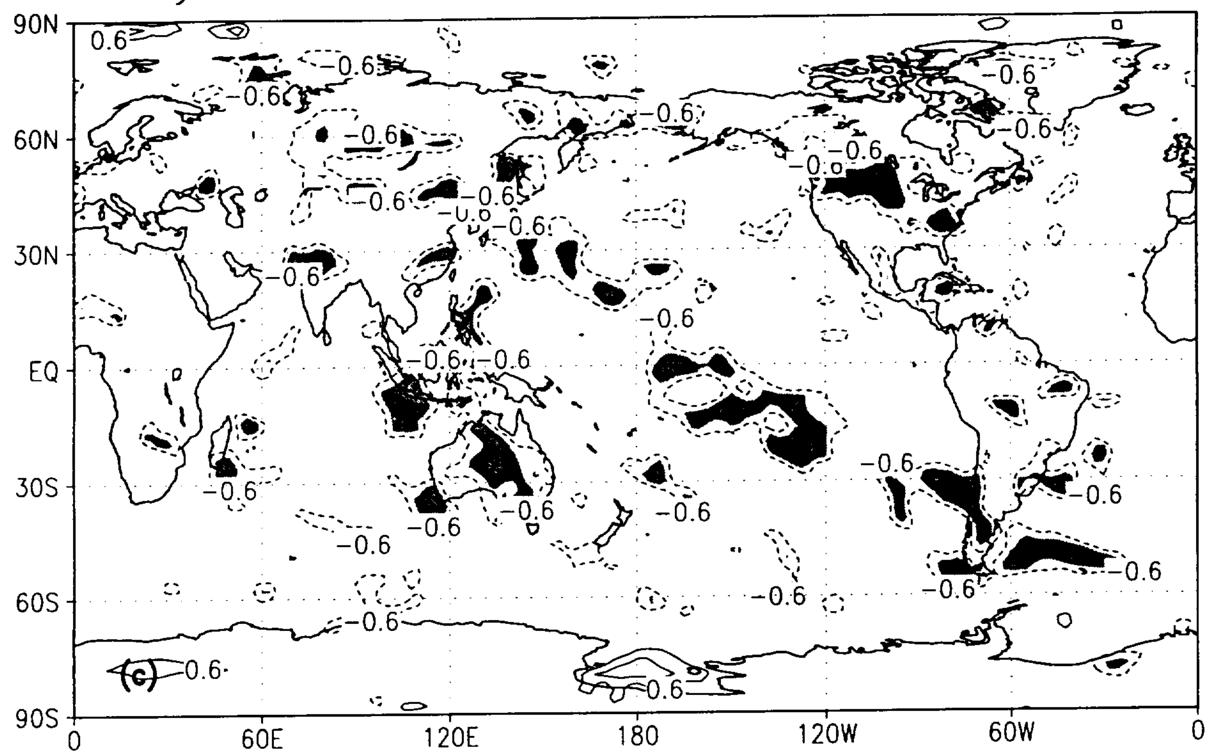

October 1986–93 corr. VAVGQLA' and OLR'

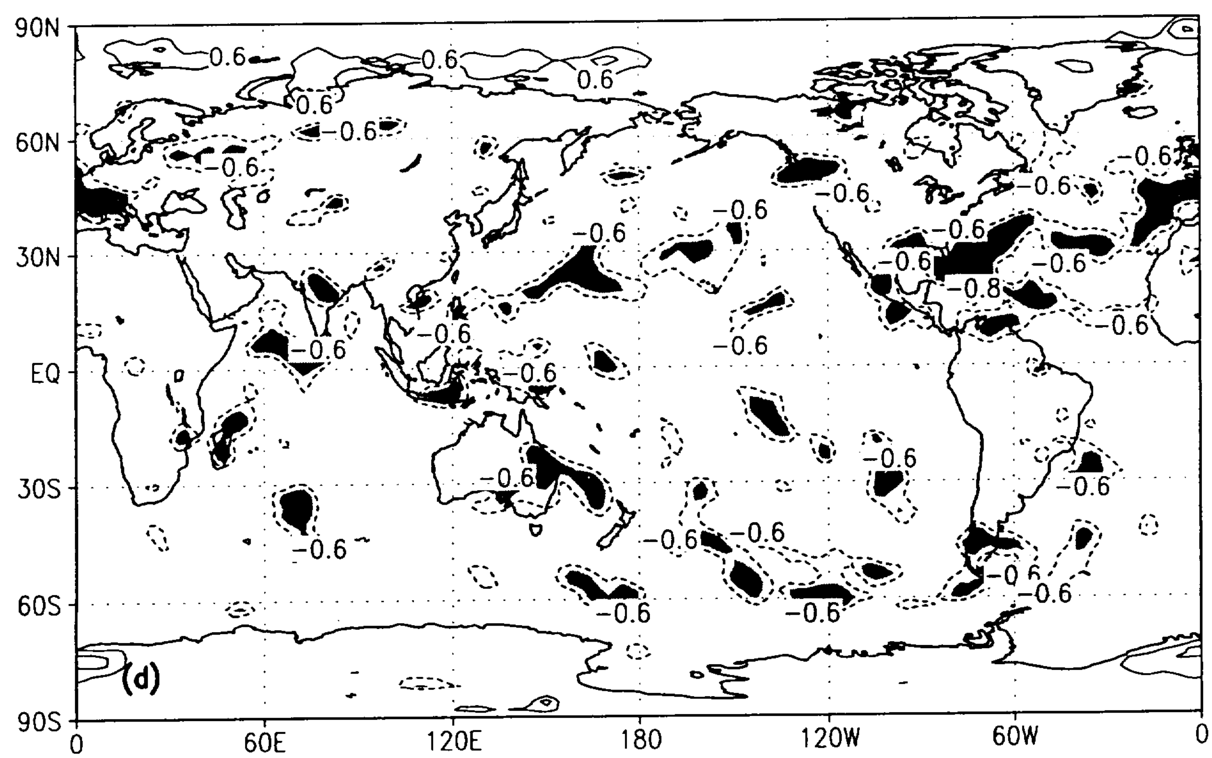

Angular momentum and energetics in reanalysis products

David A. Salstein and Richard D. Rosen
Atmospheric and Environmental Research, Inc., Cambridge, MA 02139

1. ***Introduction***. Questions about climate variability demonstrate the need to reanalyze the historical state of the atmosphere using a modern analysis system applied to as consistent a set of observational data as possible. Two such reanalysis sets are now being prepared: one by NCEP/NCAR, eventually spanning several decades (Kalnay and Jenne 1991); and one using the NASA Goddard Earth Observing System Data Assimilation System (GEOS-1 DAS), being run for about a decade but developed with future inputs of space-based data in mind (Schubert et al. 1991).

The currently available pilot series from these reanalyses span more than five years. Here we examine the potential for these data to contribute to climate studies by considering aspects of the planetary budgets of atmospheric angular momentum and energetics.

2. ***Angular momentum diagnostics***. Atmospheric angular momentum (AAM) about Earth's axis is a well-determined quantity, which has been shown to be remarkably consistent with measurements of the Earth's rotation rate in that its variations are proportional to those in the length of day (l.o.d.) on timescales between several days and years. In addition, AAM is being used as a verification tool for atmospheric models (Salstein and Rosen 1994) such as those contributing to the Atmospheric Model Intercomparison Project. Estimates of this quantity have been made from several weather centers (Salstein et al. 1993), and although values produced by different centers had moderate differences a decade or more ago, they are in better agreement today. New estimates of AAM based on reanalyses have the potential to reduce the errors that existed in earlier years.

The difference between AAM and equivalent values of l.o.d. for individual years is typically smaller when the AAM value is based on NCEP/NCAR reanalysis than when it is derived from operational analyses. Indeed, a seven-year set (1985-91) of values shows the reduction in rms to be about 30%; this result (Fig. 1) was determined using the full vertical extent of the analysis domains and after removing a low-order signal not related to atmosphere-solid Earth momentum exchange.

The differences in AAM between reanalyses and operational analyses appear to derive from zonal winds in the tropics and southern hemisphere mid to high latitudes. Reanalysis appears to have stronger easterly momentum than do operational values, in general. Interestingly also, reanalysis-based AAM values are temporally smoother than their operational counterparts, as a spectral analysis of such values over the five years demonstrates (Fig. 2).

An advantage of reanalysis data derives from the inclusion of higher levels than was the case heretofore. Use of such levels is typically required for momentum balances on seasonal scales (Rosen and Salstein 1991). For example, the semiannual amplitude in l.o.d. of 0.173 milliseconds during 1985-91 is not matched by the troposphere alone (amplitude equivalent to 0.116 ms), but including of the stratosphere up to the 20 millibar level reduces the difference with the l.o.d.-derived value by about one half (amplitude equivalent to 0.144 ms).

Values of AAM, when distributed into zonal belts, can be used to study the structure of climate anomalies. The GEOS-1 system, for example, shows the 1987 El Niño maximum and 1988 La Niña minimum in the subtropics, each signal with a precursor near the equator one year earlier.

Such a result, first noted by Dickey et al. (1991), may eventually be generalized over many decades with the reanalysis-based values.

NCEP/NCAR and NASA GEOS-1-based values of AAM are in rather close agreement with each other, with the two sets showing a strong coherence on intraseasonal time scales that remains statistically significant down to about three days (Fig. 3). From this result, we may infer that the reanalysis sets have consistent zonal wind fields.

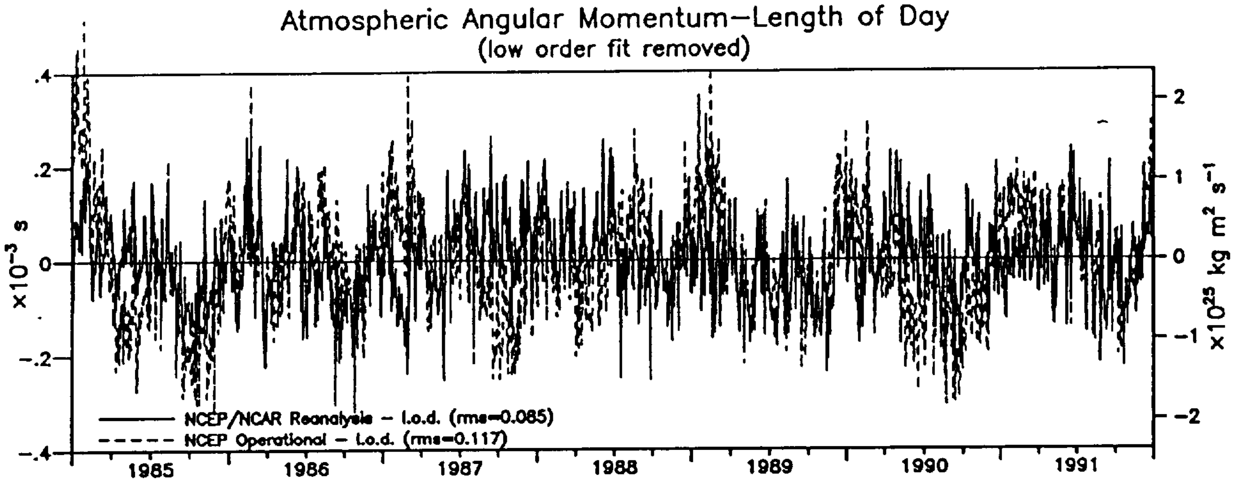

Fig. 1. Difference between AAM and equivalent length of day values, given in two proportional scales, l.o.d. on left and AAM on right. AAM is derived from NCEP/NCAR reanalyses and NCEP operational analyses. A low-order fit, representing non-atmospheric effects, is removed from the difference series.

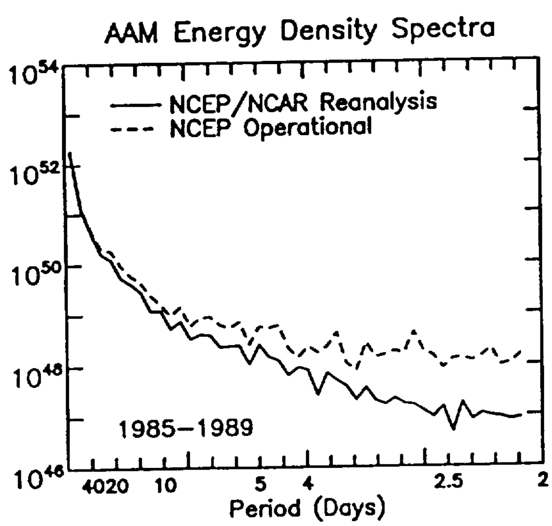

Fig. 2. Energy density spectra of AAM from NCEP/NCAR reanalyses and NCEP operational analyses for 1985-1989, based on once-daily values. Units are (kg m^2 $s^{-1})^2$ x day.

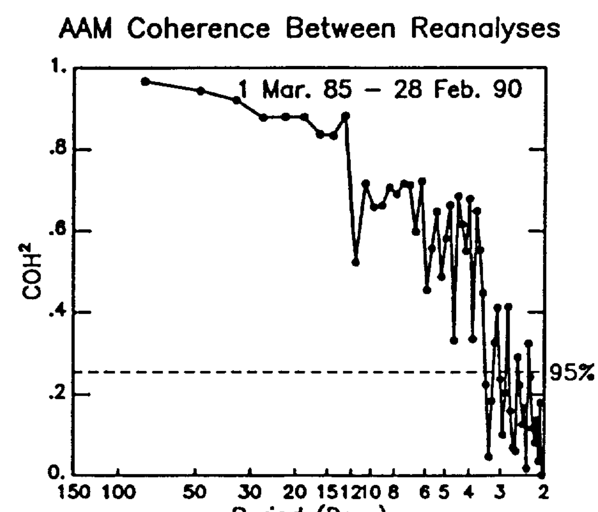

Fig. 3. Square of coherence between AAM values (to 20 millibars) from the NCEP/NCAR and NASA GEOS-1 DAS reanalyses over five years,and an estimate of the 95% level of significance.

3. ***Energy diagnostics***. The atmosphere may be considered as a heat engine in which potential energy is converted into kinetic energy (Peixoto and Oort 1992). Moreover, these energy forms may be partitioned into their zonal mean and eddy components, with conversions taking place between such components by actions of meridional eddy transports. Potential energy is generated through differential heating of the atmosphere through diabatic processes; the generation of its zonal mean form, for example, requires a positive correlation of heating rate and temperature across the (hemispheric or global) domain. The diabatic processes involved are those of sensible, latent, longwave radiational, and shortwave radiational heating.

Signals in the strength of atmospheric energy forms, conversions, and generation can be indicative of important interannual variations. We used the first five years of the NASA GEOS-1 analysis to analyze atmospheric energetics in monthly periods. Potential and kinetic energy contents of each hemisphere display strong annual signals, with all zonal mean and eddy components strongest during a hemisphere's winter. Furthermore, the northern hemisphere signal dominates the seasonal signal. When the mean seasonal cycle is removed, the transition from 1987 El Niño maximum to 1988/1989 La Niña minimum is clearly visible in the energy signals in both hemispheres (Fig. 4). The time series of zonal mean available potential energy generation displays a signal in which the portion associated with latent heat explains much of the character of total energy generation (Salstein and Sud 1994). Moreover, interannual signals in anomaly generation terms also indicate an impact of the ENSO cycle.

We have also made a preliminary estimate of the differences in the energetics between the NCEP/NCAR and GEOS-1 DAS reanalyses during the 1987-1988 period, which are relatively small (only 5% or less of the typical values). Some of the larger differences are in the zonal mean available potential energy in the southern hemisphere and eddy kinetic energy in both hemispheres, in which the NCEP/NCAR values tend to be less than those of GEOS-1 DAS. After examining zonal-mean zonal wind values, we find, for March 1988, the month with the largest difference in mean kinetic energy, that such a difference is related to the strength and position of the jets, which tend to be stronger and placed more equatorward in the NCEP/NCAR analysis. As for eddy kinetic energy, the two-year mean conditions show that the zonal mean variance in the winds in NCEP/NCAR is less than that of GEOS-1 throughout much of the globe, but in particular in the southern hemisphere jet, which is centered near 50S and 250 millibars (Fig. 5).

4. *Acknowledgments*. Support for this study came from NOAA Climate and Global Change Program grant NA46GP0212, and from NASA EOS Program grant NAGW-2615 and Global Modeling and Analysis Program contract NAS5-32861.

5. ***References***

Dickey, J. O., S. L. Marcus, and R. Hide, 1992: Global propagation of interannual fluctuations in atmospheric angular momentum. *Nature*, 357, 484-488.

Kalnay, E. and R. Jenne, Summary of the NMC/NCAR reanalysis workshop of April 1991. *Bull. Amer. Metoeorol. Soc.*, 72, 1897-1904.

Peixoto, J.P., and A.H. Oort, 1992: *Physics of Climate*, Amer. Inst. Phys., New York, 520 pp.

Rosen, R.D., and D.A. Salstein, 1991: Comment on "A seasonal budget of the Earth's axial angular momentum" by Naito and Kikuchi. *Geophys. Res. Lett.*, 18, 1925-1926

Salstein, D.A., D.M. Kann, A.J. Miller, and R.D. Rosen, 1993: The Sub-bureau for Atmospheric Angular Momentum of the International Earth Rotation Service: A meteorological data center with geodetic applications. *Bull. Amer. Meteorol. Soc.*, 74, 67-80.

Salstein, D.A., and R.D. Rosen, 1994: Validation of model-based and analyzed momentum and moisture diagnostics. *Proc. 19th NOAA Climate Diagnostics Workshop*, College Park, MD.

Salstein,D.A., and Y. Sud.1994: Large-scale diabatic heating in a model with downdrafts. *Proc. 10th Conf. on Numerical Weather Prediction*, Amer. Meteror. Soc., 72-74.

Schubert, S. D., R.B. Rood, and J. Pfaendtner, 1993: An assimilated dataset for Earth science applications. *Bull. Amer. Meteorol. Soc.*, 74, 2331-2342.

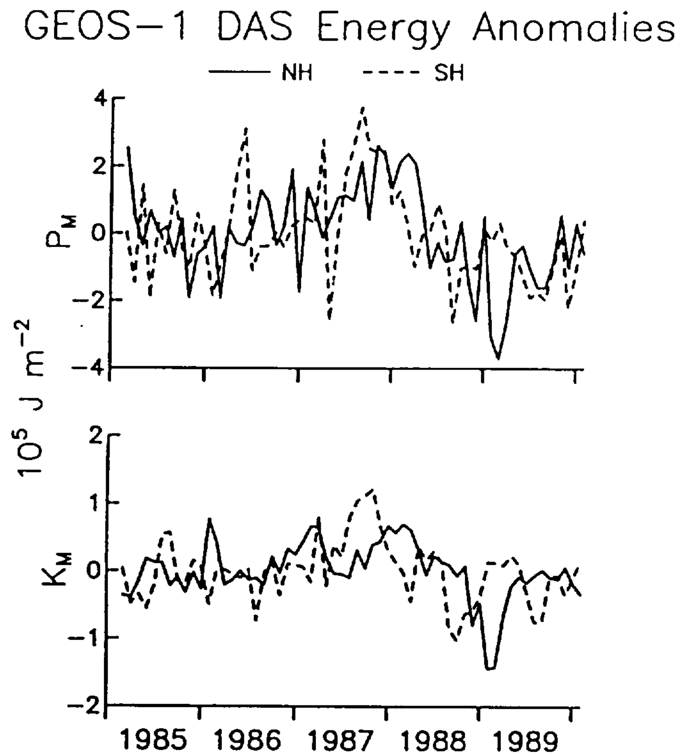

Fig. 4. Hemispheric anomaly values from five-year calendar-monthly means for zonal mean potential and zonal mean kinetic energies, based on the NASA GEOS-1 DAS system.

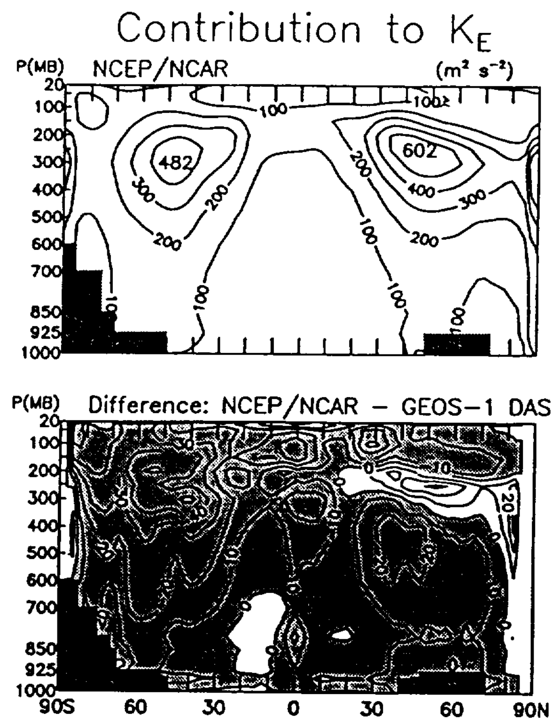

Fig. 5. Pressure-latitude distribution, 1987/88 of the mean square transient and standing eddy wind components from one reanalysis and from the difference between two reanalyses. Values are proportional to eddy kinetic energy. Light and dark shading represent negative values and high topography regions respectively.